Alma Mater Studiorum · Università di Bologna

Dipartimento di Fisica e Astronomia "Augusto Righi"
Corso di Laurea in Fisica

Measurement of ΔA_{CP} using semileptonic charm baryons decays at LHCb

Relatore:
Prof. Angelo Carbone

Correlatore:
Dott. Francesco Zenesini

Presentata da:
Federico Bonfè

Anno Accademico 2023/2024

Abstract

In the observable universe, matter dominates on antimatter. Among the necessary conditions for this asymmetry to occur, there are CP violations, which are measurable as differences between the decay rate of a particle and that of the corresponding antiparticle, once a certain final state is fixed. The Standard Model (SM) can describe this phenomenon, but the amount of CP violation that is calculated is insufficient alone, hence there must be also other sources. New theories formulated beyond the SM need experimental measurements to prove their predictions. At CERN in Geneva, the LHCb experiment is carried on with the purpose of quantifying the amount of CP asymmetry in the decays of beauty and charmed hadrons. In this thesis work it is calculated the difference between the CP asymmetries in the decay channels $\Lambda_c^+ \to p + K^+ + K^-$ and $\Lambda_c^+ \to p + \pi^+ + \pi^-$ of the charmed baryon Λ_c^+. The presented analysis uses Run 2 data, collected by the LHCb experiment in 2016, obtained from proton-proton collisions at center-of-mass energies of $\sqrt{s} = 13$ TeV, with an integrated luminosity of 0.82 fb^{-1} and magnet down polarity. This analysis was already performed during Run 1 and has measured $\Delta A_{CP}^{wgt} = (0.30 \pm 0.91 \pm 0.61)\%$, where the first uncertainty is statistical and the second is systematic. This work aims to futher study this decays with the higher statistics of Run 2. From the data sample the two raw asymmetries $A_{raw}(pK^+K^-)$ and $A_{raw}(p\pi^+\pi^-)$ are measured. However, nuisance asymmetries, such as the production asymmetry of the charm baryon $\Lambda_c^+$and the detection asymmetry of the proton can bias the raw asymmetry, thus effectively making them different from CP asymmetries. Nuisance asymmetries are assumed to depend only on the kinematics of the final state. The events referring to $\Lambda_c^+ \to p + \pi^+ + \pi^-$ channel are weighted so that the kinematics of Λ_c^+ and p match the kinematics of the same particles in the other channel, $\Lambda_c^+ \to p + K^+ + K^-$. The following results are obtained,

$$A_{raw}(pK^+K^-) = (2.4 \pm 0.8)\%,$$

$$A_{raw}^{wgt}(p\pi^+\pi^-) = (2.6 \pm 0.5)\%.$$

The weighting procedure ensures that nuisance asymmetries contained in $A_{raw}(pK^+K^-)$ and $A_{raw}^{wgt}(p\pi^+\pi^-)$ can be assumed equal. This implies that they cancel out when the difference $A_{raw}(pK^+K^-) - A_{raw}^{wgt}(p\pi^+\pi^-)$ is calculated, so that it corresponds to the difference between the two CP asymmetries in the decay, i.e. $A_{raw}(pK^+K^-) - A_{raw}^{wgt}(p\pi^+\pi^-) \approx A_{CP}(pK^+K^-) - A_{CP}^{wgt}(p\pi^+\pi^-) \equiv \Delta A_{CP}^{wgt}$. The estimated value is

$$\Delta A_{CP}^{wgt} = (-0.2 \pm 0.9)\%,$$

where only the statistical uncertainty is reported, while systematic uncertainties will be studied in the future. The results are compatible with the hypothesis of CP conservation in these decays and with Run 1 measurements.

Abstract

Nell'universo osservabile la materia domina sull'antimateria. Tale asimmetria è causata dalle violazioni di CP, misurabili come una differenza tra il tasso di decadimento di una particella e della corrispondente antiparticella, fissato un determinato stato finale. Il Modello Standard (MS) è in grado di descrivere tale fenomeno, ma l'entità che vi attribuisce è insufficiente da sola, perciò devono esistere anche altre fonti di violazione di CP. Le nuove teorie formulate oltre il MS necessitano però di misurazioni sperimentali che ne possano verificare le previsioni. Al CERN di Ginevra viene portato avanti il progetto LHCb proprio con lo scopo di quantificare le asimmetrie di CP nei decadimenti di adroni contenenti quark beauty e charm. In questo lavoro di tesi viene calcolata la differenza tra le asimmetrie di CP nei due canali di decadimento $\Lambda_c^+ \to p+K^++K^-$ e $\Lambda_c^+ \to p+\pi^++\pi^-$. L'analisi che viene presentata utilizza dati di Run 2, raccolti dall'esperimento LHCb nel 2016 e ottenuti da collisioni protone-protone ad una energia del centro di massa pari a $\sqrt{s} = 13$ TeV, con una luminosità integrata di 0.82 fb^{-1} e con magdown. Questa analisi è già stata eseguita durante Run 1, ottenendo come misura $\Delta A_{CP}^{wgt} = (0.30 \pm 0.91 \pm 0.61)\%$, dove la prima è l'incertezza statistica, la seconda è l'incertezza sistematica. Dal campione di dati si possono ricavare le due asimmetrie grezze $A_{raw}(pK^+K^-)$ e $A_{raw}(p\pi^+\pi^-)$. Tuttavia, le asimmetrie di disturbo, come l'asimmetria di produzione del barione charm $Lambda_c^+$and l'asimmetria di rilevamento del protone possono influenzare l'asimmetria grezza, rendendole così effettivamente diverse dalle asimmetrie CP. Si presume che le asimmetrie di disturbo dipendano solo dalla cinematica dello stato finale. Gli eventi che si riferiscono al canale $\Lambda_c^+ \to p + \pi^+ + \pi^-$ sono stati quindi pesati in modo tale che le cinematiche della Λ_c^+ e del protone corrispondessero alle cinematiche delle medesime particelle nell'altro canale, $\Lambda_c^+ \to p + K^+ + K^-$. In seguito a ciò i risultati ottenuti sono

$$A_{raw}(pK^+K^-) = (2.4 \pm 0.8)\%,$$

$$A_{raw}^{wgt}(p\pi^+\pi^-) = (2.6 \pm 0.5)\%.$$

La procedura di ripesaggio fa sì che gli errori sistematici contenuti in $A_{raw}(pK^+K^-)$ e in $A_{raw}^{wgt}(p\pi^+\pi^-)$ si possano ritenere uguali. Ciò implica che si cancellano nel momento in cui viene calcolata la differenza $A_{raw}(pK^+K^-) - A_{raw}^{wgt}(p\pi^+\pi^-)$, cosicché quest'ultima corrisponde circa alla differenza tra le due asimmetrie di CP, cioè $A_{raw}(pK^+K^-) - A_{raw}^{wgt}(p\pi^+\pi^-) \approx A_{CP}(pK^+K^-) - A_{CP}^{wgt}(p\pi^+\pi^-) \equiv \Delta A_{CP}^{wgt}$. Il valore così ottenuto è

$$\Delta A_{CP}^{wgt} == (-0.2 \pm 0.9)\%.$$

dove viene riportata soltanto l'incertezza statistica, mentre le incertezze sistematiche verranno studiate in futuro. I risultati sono compatibili con l'ipotesi della conservazione di CP in questi decadimenti e con le misre di Run 1.

Dedications

Dedico questa tesi
alla Sara, alla Micia,
al Gatto Rosso e al Gatto Nero,
che hanno studiato insieme a me.
E per finire, "sempre forza Simo!".

Acknowledgements

Desidero ringraziare il Prof. Angelo Carbone per la preziosa opportunità che mi ha dato.

Un grazie speciale al Dott. Francesco Zenesini, per l'energia e il tempo dedicati al progetto, per l'aiuto e le cose che ho imparato.

Contents

Introduction

Nowadays in the universe, a large asymmetry is observed between the amount of matter and antimatter. Nevertheless, at a fundamental level, both production and annihilation processes always involve a particle-antiparticle pair. In addition, it is believed that after the Big Bang the same amount of matter and antimatter were created. These two facts would lead to the opposite expectation, i.e. a universe in which matter and antimatter are present in equal proportions until only massless photons are left, via processes such as $e^+ + e^- \to \gamma\gamma$. However, since this latter scenario is rejected by evidence, the behaviours of matter and antimatter must be somehow different. This was effectively measured in CP-violating decays, where particles decay at a different rate with respect to the corresponding antiparticle.

The Standard Model (SM) is the currently accepted and most complete theory. It is capable of good predictions involving strong, weak and electromagnetic interactions, which are described within the quantum field theory framework. The only fundamental interaction left out is the gravitational force. The SM further classifies the elementary particles that have been discovered until today, which are listed in Fig. 1. The particle types can be divided into

- quarks,
- leptons,
- force carriers,
- the Higgs boson.

Matter particles can be either quarks or leptons; both are fermions with spin $s = \frac{1}{2}$. They differ because quarks can undergo all four kinds of interactions, whereas leptons do not have a color charge and so they cannot be affected by the corresponding force, the strong force. The photon, the W and Z bosons, and the gluon are the force carriers, i.e. the mediators of the forces, which couples to the matter particles with intensity (probability) proportional to the charge of these latter. The force carriers are bosons with spin $s = 1$. The Higgs boson instead has spin $s = 0$, and its coupling to $W^\pm$, Z bosons makes them massive without breaking gauge symmetries, which instead require them to be massless in order to describe the interactions correctly.

The SM provides a source of CP violation. However, the amount of CP violation that can be predicted is not large enough to justify the asymmetry between matter and antimatter in our universe. LHCb experiment has been designed to measure CP asymmetries in beauty and charmed hadron decays, so as to look for discrepancies from the values of asymmetry predicted within the SM, which would result in evidence of new physics, beyond the SM. These measurements could then be used either to prove or to falsify new theories, that are necessary to explain the almost total absence of antimatter in today's universe.

In the complex frame above described, the purpose of this thesis work is to measure the different CP asymmetries between two decay channels of the charmed baryon Λ_c^+, specifically $\Lambda_c^+ \to p + K^+ + K^-$ and $\Lambda_c^+ \to p + \pi^+ + \pi^-$.

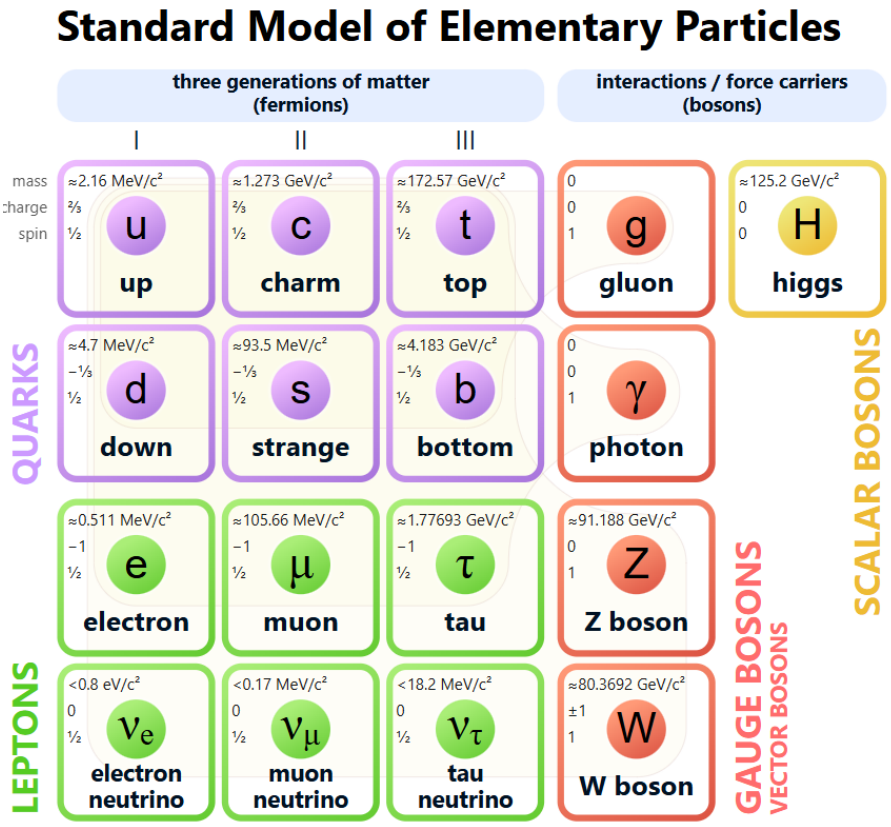

Figure 1: Elementary particle types of the Standard Model.

Chapter 1

Theoretical framework

1.1 Transformations and symmetries

"A symmetry is a transformation that can be performed on a system that leaves its physical description unchanged"[1]. The physical description is nothing but the mathematical law that governs the evolution of that system, which after that specific symmetry transformation is either precisely identical or, in general, at least keeps the same form; in the first case the equation is said to be invariant, while in the second case it is called covariant, or invariant in form. For instance, according to Einstein's restricted theory of relativity, all physical laws must be 'the same' in every inertial frame of reference, i.e. symmetric under Lorentz transformations. It implies that all equations must be formed out of scalars and tensors. Scalars are invariant under Lorentz transformations, i.e. same value and sign in every frame. Tensors are defined by the property that they transform under Lorentz in a specific way that is exactly the same for all tensors of the same type, thus leaving the form of the equation unaltered.

A set of symmetry transformations is called a group, with respect to a given composition (multiplication) operation, if it includes the identity element and an inverse for every element of the set, and if it further verifies the associative and closure properties. This latter is crucial since it means that the multiplication of any two elements of the set is still an element that belongs to the set. The restricted group of Lorentz transformations $SO^{+}(1,3)$, together with space-time translations, forms the Poincaré group, which is the basis of particle physics, since all fundamental particles are described using its representations. A distinction can be made between transformations: the elements of a group that depend on parameters which can vary continuously over a certain range are called continuous transformations, such as rotations of a circle, or a sphere; on the contrary, if the set of symmetries is finite or countable, they are called discrete transformations.

Symmetries are fundamental in particle physics, their importance became clearer in 1918 when E. Noether published what has become famous as Noether's theorem[2]. It

states that to every continuous symmetry of a physical system corresponds the conservation of some quantity as that system evolves in time. Both the possible approaches to this theorem can be extremely helpful. On one side, assuming some symmetries of the system, a Lagrangian can be built that reflects these properties and so new interactions come out, whose real existence can be validated through experiments. Such experiments have to verify whether the quantities whose conservation is implied by Noether's theorem are actually constant in time. This is what happened for example when it was understood that electromagnetic interactions are $SU(1)$ local gauge interactions ($U(1)$ to be precise), i.e. they are retrieved when a $SU(1)$ local gauge symmetry is required starting from the theory of free particles. So, in analogy to this, $SU(2)$ and $SU(3)$ local gauge interactions were built imposing the symmetries; these resulted to describe correctly weak and strong interactions respectively. On the other side, the empirical validation of the conservation of some quantities in a certain physical system imposes rigid constraints on the terms that can appear in the Lagrangian, thus simplifying its writing.

Some examples of correlations that can be obtained using Noether's theorem are three-momentum conservation from spatial translation invariance, energy conservation from time translation invariance and angular momentum from rotational invariance. These have been proven true all the times, up to now, and thus express some properties of the space-time which are called respectively spatial and temporal homogeneity and spatial isotropy. Those presented above, coming from Poincaré group, were all examples of exact symmetries, which lead to conservation laws that must be fulfilled by all processes in a fixed frame of reference. There is another important class of so called approximate symmetries, which are valid only under specific conditions or making the hypothesis of considering only a partial physics. For instance, at low speed, $\frac{v}{c} \ll 1$, when relativistic effects are negligible, the conservation of mass becomes true; otherwise, assuming to deal only with strong interactions, the opposite electric charge of up and down quark is irrelevant, and the "accidental" small difference of their masses makes it possible to mix them, e.g. to "rotate" up quarks into down quarks or into any linear combination of the two, without a change in the strong interaction that occurs. This is called isospin symmetry and leads to the conservation of the quantum number I.

Noether's theorem is not valid for discrete symmetries, but despite that, when a discrete symmetry is verified, still there is a conserved quantity. In turn it is discrete and it must be conserved throughout time evolution; thus, in particle physics if such symmetries exist for a given initial state of particles, they give the possibility to distinguish between final states in which the system might be found in the future, and those in which may not, i.e. between processes with non-zero and zero amplitude. To summarize, these numbers act as selection rules.

In the next section, parity, charge conjugation and time reversal transformations will be presented. At first, it was believed that these discrete symmetries were preserved by all three fundamental interactions; however, all of them have been proven violated by weak interactions, as it will be discussed later. Consequently, parity, charge conjugation

and time reversal parities, when defined, are conserved under electromagnetic and strong interactions only.

1.2 Parity, charge conjugation, time reversal

The restricted Lorentz group $SO^+(1,3)$ is a subgroup of the Lorentz group $O(1,3)$ that takes into consideration only those transformations which satisfy $\Lambda^\mu_\rho \eta^{\rho\sigma} \Lambda^\nu_\sigma = \eta^{\mu\nu}$ along with a positive determinant, equal to +1, and $\Lambda^0_0 > 0$. Some of the left out transformations, those not special, are for example spatial parity, given by diag(1,-1,-1,-1), or time reversal, given by diag(-1,1,1,1), both in fact have determinant equal to -1.

- Parity is the transformation that inverts all three spatial axes at once. It is equivalent to the reflection of one axis combined with a 180° rotation around that axis. The action of such transformation, represented by the operator $\hat{P}$, on a position three-vector $\vec{x}$ is

$$\hat{P}\vec{x} = -\vec{x}, \tag{1.1}$$

  which results in the negated position vector; likewise for all other proper vectors, such as the velocity. This can be easily understood considering its definition, $\vec{v} \equiv \frac{d\vec{x}}{dt}$. On the contrary, pseudo-vectors, defined by the vector product of two proper vectors, are invariant under parity transformation; the example of the orbital angular momentum $\vec{l} \equiv \vec{x} \times \vec{p}$ can be made:

$$\hat{P}\vec{l} = \hat{P}(\vec{x} \times \vec{p}) = \hat{P}\vec{x} \times \hat{P}\vec{p} = (-\vec{x}) \times (-\vec{p}) = \vec{x} \times \vec{p} = \vec{l}. \tag{1.2}$$

- Charge conjugation inverts all the internal charges, transforming particles into their anti-particles and vice versa. It is applied using the operator $\hat{C}$. Charge conjugation acts only on some internal degrees of freedom and it does not belong to the O(1,3) group, differently from parity and time reversal transformations. It is important to stress that "the action of charge conjugation does nothing to spin. Therefore, its action on spinors is to turn particles into antiparticles without affecting the helicity of that particle"[1].

- Time reversal is the third important discrete transformation, its action is represented by the operator $\hat{T}$, such that

$$\hat{T}t = -t. \tag{1.3}$$

  The position vector is unchanged under time reversal,

$$\hat{T}\vec{x} = \vec{x}, \tag{1.4}$$

whereas the speed vector and the angular momentum are flipped,

$$\hat{T}\vec{v} = -\vec{v} \quad \text{and} \quad \hat{T}\vec{l} = -\vec{l}. \tag{1.5}$$

In fact, using the definition of velocity,

$$\hat{T}\vec{v} = T\frac{d\vec{x}}{dt} = \frac{d\vec{x}}{d(-t)} = -\frac{d\vec{x}}{dt} = -\vec{v}. \tag{1.6}$$

Consequently

$$\hat{T}\vec{l} = \hat{T}(\vec{x} \times m\vec{v}) = \hat{T}(\vec{x}) \times m\hat{T}(\vec{v}) = \vec{x} \times m(-\vec{v}) = -\vec{l}. \tag{1.7}$$

1.2.1 CPT theorem

It can be verified that electromagnetism is invariant under parity, charge conjugation and time reversal transformations. The four Maxwell equations are:

$$\vec{\nabla} \cdot \vec{E} = \rho, \qquad \vec{\nabla} \times \vec{E} = -\frac{\partial \vec{B}}{\partial t}, \tag{1.8}$$

$$\vec{\nabla} \cdot \vec{B} = 0, \qquad \vec{\nabla} \times \vec{B} = \vec{J} + \frac{\partial \vec{E}}{\partial t}.$$

Consider the effect of $\hat{P}$, $\hat{C}$, $\hat{T}$ transformations on each component separately:

$$\hat{P}\vec{E} = -\vec{E}, \quad \hat{P}\vec{\nabla} = -\vec{\nabla}, \quad \hat{P}\rho = \rho, \quad \hat{P}\vec{B} = \vec{B}, \quad \hat{P}\vec{J} = -\vec{J}, \quad \hat{P}\frac{\partial}{\partial t} = \frac{\partial}{\partial t}. \tag{1.9}$$

$$\hat{C}\vec{E} = -\vec{E}, \quad \hat{C}\vec{\nabla} = \vec{\nabla}, \quad \hat{C}\rho = -\rho, \quad \hat{C}\vec{B} = -\vec{B}, \quad \hat{C}\vec{J} = -\vec{J}, \quad \hat{C}\frac{\partial}{\partial t} = \frac{\partial}{\partial t}. \tag{1.10}$$

$$\hat{T}\vec{E} = \vec{E}, \quad \hat{T}\vec{\nabla} = \vec{\nabla}, \quad \hat{T}\rho = \rho, \quad \hat{T}\vec{B} = -\vec{B}, \quad \hat{T}\vec{J} = -\vec{J}, \quad \hat{T}\frac{\partial}{\partial t} = -\frac{\partial}{\partial t}. \tag{1.11}$$

If the new, transformed quantities are plugged into the equations, the same equations are re-obtained. Based on this, up until the 50's it was believed that all fundamental interactions had to have these three independent symmetry properties; however, in the next sections it will be shown that this belief fell down.

What can be effectively proven is the so called CPT theorem. It states that the composition of all three transformations is an exact symmetry of any system described by an Hermitian Hamiltonian operator $\hat{H}$, which can be mathematically translated as

$$\hat{C}\hat{P}\hat{T}\hat{H} = \hat{H}^{\dagger}. \tag{1.12}$$

Thus, symmetries can be singularly violated, as long as the action of $\hat{C}\hat{P}\hat{T}$ is preserved. For instance, suppose that both P , C symmetry are individually broken: if their combination restores symmetry, then as consequence of CPT theorem the T symmetry is preserved. However, CP symmetry can be violated too in principle, then in turn it becomes necessary for T symmetry to be broken as well to obtain back CPT symmetry.

1.3 Decays and interactions

The matrix element $A_{fi} \equiv \langle f|H_{int}|i\rangle$ gives the transition amplitude of the decay of a certain particle in the initial state i into n particles described by a final state f, governed by the interaction Hamiltonian H_{int}. The energies and momenta of all the particles have a definite value in the computation of a matrix element. Once the reference frame is fixed, the initial particle has energy E and momentum $\vec{p}$; so, in order to compute the decay rate to a final state of n specified particles, one has to integrate over all possible kinematic configurations of the n decay products, i.e. those combinations that respect the conservation of energy and momentum. This considered, the final expression for the decay rate, i.e. "the probability of transition per unit time to the final state f of n particles is"[3]

$$\Gamma_{if} = \frac{1}{2E}\int |A_{fi}|^2 (2\pi)^4 \prod_{i=1}^{n} \frac{d^3p_i}{(2\pi)^3 2E_i} \delta\left(\sum_{i=1}^{n} E_i - E\right) \delta^{(3)}\left(\sum_{i=1}^{n} \vec{p_i} - \vec{p}\right), \tag{1.13}$$

where E is the energy of the initial particle, while E_i is the energy of the $i-th$ final particle. The integral in momentum space is made over all possible combinations of energies and momenta of the final products that respect conservation laws. Further, the matrix elements can be evaluated using the Standard Model. The total decay rate for a given particle is obtained summing over all possible branches, i.e. the accessible final states distinct for type and number of the products. The branching ratio is defined as the ratio of that specific branch divided by the total decay rate.

Considering interactions, the only difference with respect to decays is that the initial state is composed of two particles, each with fixed energy and momentum. A quantification of the probability for an interaction to produce n specific particles can be obtained calculating its cross section, whose expression is in perfect analogy with that of a decay rate,

$$\sigma_{if} = \frac{1}{2E_a 2E_b |\vec{\beta}_a - \vec{\beta}_b|}\int |A_{fi}|^2 (2\pi)^4 \prod_{i=1}^{n} \frac{d^3p_i}{(2\pi)^3 2E_i} \delta\left(\sum_{i=1}^{n} E_i - (E_a + E_b)\right) \delta^{(3)}\left(\sum_{i=1}^{n} \vec{p_i} - (\vec{p_a} + \vec{p_b})\right), \tag{1.14}$$

In the simple case of an elastic scattering process $a + b \to a + b$, in non-relativistic regime, the transition amplitude can be calculated considering that the particle a with charge g interacts with the potential field $g_0\phi$, where g_0 is the charge of particle b, which generates this potential. The particle a in the initial and final states, far from b, can be considered free, and so its propagation in space is well-described by the plane waves ψ_i, ψ_f. To make calculations easier one can assume that the mass M of b is much greater than the mass of a, thus b results unaffected by the interaction. Moreover, one can take the Yukawa potential of range $1/m$ to describe a short-range interaction, such as weak interactions, where m is the mass of the carrier of the force. Eventually, the following

result is obtained

$$\langle \psi_f | g_0 \phi | \psi_i \rangle = \frac{g_0 g}{|\vec{q}|^2 + m^2}, \tag{1.15}$$

where $\vec{q}$ is the three-momentum transferred $\vec{q} \equiv \vec{p}_2 - \vec{p}_1$.

Moving to the relativistic regime and dropping the condition that the mass of b is much greater than the mass of a, the expression for the matrix element, i.e. the scattering amplitude, becomes

$$\langle \psi_f | g_0 \phi | \psi_i \rangle = \frac{g_0 g}{m^2 - t}, \tag{1.16}$$

where t is the norm of the four-momentum transferred, $t \equiv (E_2 - E_1)^2 - (\vec{p}_2 - \vec{p}_1)^2$ and m is the mass of the boson V. At quantum level, particles a and b interact exchanging energy and momentum via a field quantum V that is a force carrier, as represented in Fig. 1.1. Note that the expression for the scattering amplitude contains three factors. The first is g, which furnishes the probability for the emission of the boson V, i.e. that the matter field of quantum a couples to the force field. The second is $\frac{1}{m^2-t}$, which expresses the probability for the carrier to move from a to b. Finally, g_0, analogously to g, represents the probability for the absorption of V, i.e. that the force field couples to the second matter field.

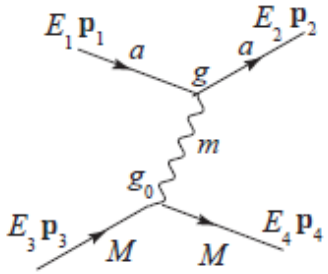

Figure 1.1: Feynman diagram of the elastic scattering of two particles.

When using the Feynman diagrams it is assumed that at every vertex energy and momentum are conserved. The drawback is that the four-momentum transferred does not correspond to the physical mass m of the mediator particle V, which in fact is called a 'virtual particle'; due to uncertainty principle it can live and propagate only for a limited amount of time.

1.4 Weak interactions and Cabibbo matrix

In 1934, Fermi theorized a first description of weak interactions based on the evidence of β-decays of neutrons and protons, describing them as:

$$p \to n + e^+ + \nu_e \quad \text{and} \quad n \to p + e^- + \overline{\nu_e}, \tag{1.17}$$

where a particle is destroyed while three others are created, in a single-vertex contact interaction which happens with amplitude proportional to the Fermi constant G_F, independently from the coupling particles. Subsequently, this kind of interactions were modeled like electromagnetic interactions, hence introducing the charged mediators $W^{\pm}$, massive due to the extremely short range of their action.

A deeper understanding became possible after 1964, when Gell-Mann and Zweig proposed the Quark Model, identifying up, down and strange quarks as the elementary constituents of hadrons. In light of this, for instance, proton and neutron are baryons, i.e. bound states of three quarks, in the fundamental state, thus β-decays of $p(uud)$ and $n(udd)$ can be rewritten as

$$u \to d + e^+ + \nu_e \quad \text{and} \quad d \to u + e^- + \overline{\nu_e}, \tag{1.18}$$

where actually only one quark is involved, while the other two are just spectators. Fermi description is the low energy approximation of weak interactions, where the transferred momentum is too low with respect to the mass of the mediator $m = M_W$, to make the two vertices distinguishable. This is exactly the case of β-decays, since the difference in mass between up and down quarks is extremely small. The matrix element M for a weak interaction is proportional to

$$M \propto \frac{gg}{M_W^2 - t}; \tag{1.19}$$

in the limit $t \ll M_W$, it becomes

$$M \propto G_F \propto \frac{gg}{M_W^2}. \tag{1.20}$$

The universality of the coupling constant, the charge g, was largely proven in the leptonic sector, i.e. it was measured that the bosons $W^{\pm}$ couple with the same intensity to all neutrino-lepton pairs. Apparently, the same could not be concluded in quark sector, where by that time only three quarks were known. "The problem was the following. There are two types of β-decays of the strange hadrons, those that conserve strangeness and those that violate it. Whilst universality requires the corresponding matrix elements to be equal, the latter are substantially smaller than the former"[3]. Another problem was that also in the decays where $\Delta S = 0$, with higher amplitude, the coupling constant is measured to be smaller than in leptonic sector. A possible way to reconcile the universality of the coupling constant with these two problems was proposed by Cabibbo, who suggested that weak eigenstates d', s' do not correspond precisely to the mass eigenstates d, s, but rather only at first approximation. Thus, weak eigenstates are obtained performing a rotation on the mass eigenstates of a small angle θ_C, the so called Cabibbo angle (an $SO(2)$ transformation). Note that the rotation preserves the orthogonality between d' and s'. So, one can write the linear combinations that connects the two basis,

$$d' = \cos(\theta_C)d + \sin(\theta_c)s \quad \text{and} \quad s' = -\sin\theta_C d + \cos\theta_C s. \tag{1.21}$$

The two equations can also be grouped to form the Cabibbo matrix:

$$\begin{pmatrix} d' \\ s' \end{pmatrix} = \begin{pmatrix} \cos\theta_C & \sin\theta_C \\ -\sin\theta_C & \cos\theta_C \end{pmatrix} \begin{pmatrix} d \\ s \end{pmatrix}. \tag{1.22}$$

Consider two decays that share the same final state, while their initial states differ only for a down/strange quark, e.g. $\pi^- \to \mu^- + \overline{\nu_\mu}$ and $K^- \to \mu^- + \overline{\nu_\mu}$. Following Cabibbo intuition, calculations lead to a transition amplitude proportional to $g^2 \cos\theta_C$ for the former decay which conserves strangeness, and proportional to $g^2 \sin\theta_C$ for the latter which violates strangeness. Hence, a small value of θ_C can effectively explain why transitions with $|\Delta S| = 1$ are suppressed compared to those with $\Delta S = 0$, and also why even the favoured $\Delta S = 0$ decays have smaller amplitude than leptonic sector. On the other hand, these results do not violate the universality of the coupling constant, because this latter requires g to be the coupling constant between the boson W^- and the weak eigenstate, that has become d' now.

Recalling that weak interactions are local $SU(2)$ gauge interactions, they act on doublets of weak charge; from what seen so far, the following doublets can be written

$$\begin{pmatrix} \nu_e \\ e \end{pmatrix}, \quad \begin{pmatrix} \nu_\mu \\ \mu \end{pmatrix}, \quad \begin{pmatrix} u \\ \cos(\theta_C) d + \sin(\theta_C) s \end{pmatrix}. \tag{1.23}$$

This space has the same mathematical structure as spin and isospin, so the continuous symmetry implies the conservation of the so called weak isospin t and its third component t_3. By convention ν_e is assigned quantum numbers $t = 1/2$, $t_3 = +1/2$ and thus e^- has $t = 1/2$, $t_3 = -1/2$, likewise for the other doublets.

Further, in 1970, Glashow, Iliopoulos and Maiani predicted the existence of a positively charged quark, called charm and connected to s', to create a second quark doublet "complementary" to the first,

$$\begin{pmatrix} c \\ -\sin(\theta_C) d + \cos(\theta_C) s \end{pmatrix}. \tag{1.24}$$

1.5 P violation

1.5.1 $\theta - \tau$ puzzle

During the 50's two decay channels were observed whose initial states were measured to have positive charge, strangeness +1 and, within experimental errors, identical masses and lifetimes:

$$\theta^+ \to \pi^+ + \pi^0, \tag{1.25}$$

$$\tau^+ \to \pi^+ + \pi^+ + \pi^-. \tag{1.26}$$

Accurate analysis showed also that both θ^+ and τ^+ had intrinsic spin $J = 0$. Despite all these things in common, they were left indicated as θ^+ and τ^+ since the two final states of two and three pions respectively have opposite parity: $\hat{P}(\pi^+\pi^0) = +1$ while $\hat{P}(\pi^+\pi^+\pi^-) = -1$. Parity was proved to be conserved in strong and electromagnetic interactions, therefore weak interactions were thought to do so as well. A solution to the so called $\theta - \tau$ puzzle was proposed in 1956 by Lee and Yang who claimed that parity conservation in weak interactions was actually "unsupported by experimental evidence"[4] and thus suggested that "parity is not strictly conserved, so that θ^+ and τ^+ are two different decay modes of the same particle, which necessarily has a single mass value and a single lifetime"[4]. Strong interactions produce only one meson in the fundamental state with flavour quantum numbers of isospin $I = 1/2$ and non-zero strangeness that is also positively charged, the kaon $K^+(u\bar{s})$ which eventually decays because of weak interactions.

1.5.2 Wu's experiment

It is not so trivial to identify a system capable of testing parity conservation; Lee and Yang found a possible option in β-decays, more specifically in the allowed β transition of any oriented nucleus, such as ^{60}Co. Let's go through the foundations of the experiment. A ^{60}Co nucleus decays through the well-known process

$$^{60}\text{Co} \rightarrow \ ^{60}\text{Ni} + e^- + \overline{\nu}_e. \tag{1.27}$$

The ^{60}Co nucleus is known to have intrinsic angular momentum $J_{\text{Co}} = 5$ and to decay into a ^{60}Ni nucleus with $J_{\text{Ni}} = 4$; moreover, being an allowed decay the final state has total angular momentum $L = 0$. A magnetic field is applied to align the ^{60}Co nuclear spin along a preferred axis (call it z-axis), which implies $J_{z,\text{Co}} = 5$.

In fact, the nucleus has positive charge, which means that the third component of its magnetic dipole moment μ_z can be expressed as

$$\mu_z = g\frac{Ze\hbar}{2m}s_z, \tag{1.28}$$

where Z, m are the number of protons and the mass of a ^{60}Co nucleus, while g is its gyromagnetic ratio. The potential energy

$$U = -\vec{\mu} \cdot \vec{B}, \tag{1.29}$$

using $B = B_z$, can be rewritten as

$$U = -\mu_z B, \tag{1.30}$$

and substituting Eq. 1.28 into Eq. 1.30, the expression for U becomes

$$U = -g\frac{Ze\hbar B}{2m}s_z. \tag{1.31}$$

Hence, the minimum of the potential energy is obtained when s_z is positive, which means that the nuclei align their spin in the direction of the external magnetic field, i.e. along the z-axis.

Then conservation of angular momentum causes $J_{z,\mathrm{Ni}} + J_{z,e^-} + J_{z,\overline{\nu}_e} = J_{z,\mathrm{Co}} = 5$. This means that the ^{60}Ni nucleus is not flipped and, since $L = 0$, the only possibility to recover the condition imposed before is that the spins of e^- and $\overline{\nu}_e$ are aligned too, i.e. $J_{z,e^-} = J_{z,\overline{\nu}_e} = +1/2$. Hence, to summarize, the spins of all the particles point along the positive direction of the z-axis. Then, the system presents two different possible final states: one in which the electron flies towards the positive direction of z-axis, the other in which it flies towards the negative direction, as shown in Fig. 1.2.

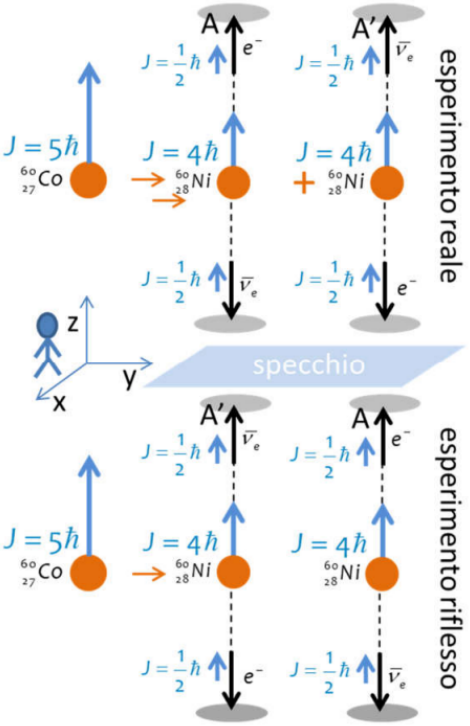

Figure 1.2: Picture illustrating the initial configuration (left) and the two possible final configurations (right), of Wu's experiment (up) and their mirror images (bottom)[5].

This system represents a good test for parity. In fact, despite doing a parity transformation, all the experimental hypotheses remain unaltered: neither the magnetic field changes orientation, nor do the nuclear spins, this because all of them are pseudo-vectors, untouched by parity. Anyhow, this does not imply that also the conclusion will be necessarily the same. In fact, the direction taken by the emitted electron is given by the orientation of its momentum, that is a vector. Under a parity transformation it flips; therefore the result is that the two possible final configurations exchange themselves.

A more concrete interpretation can be provided as well, as illustrated in Fig. 1.2: applying a parity transformation to this system is the equivalent of looking at its reflection in a mirror placed perpendicularly to the z-axis, rather than observing it directly. The "mirror" experimental set-up looks exactly the same as the real one, so the same experiment appears to be carried out, simultaneously. However, the mirror image of an electron that is flying upwards, is the same electron moving downwards instead, and vice versa.

Lee and Yang expressed formally what makes an experiment good for testing parity conservation. They wrote that there must be a pseudo-scalar, formed out of the experimentally measured quantities, that is the quantity of interest. A pseudo-scalar is a quantity that such as a scalar is invariant under rotations but, unlike it, changes sign under parity transformation. For example, "if a momentum $\vec{p}$ and a spin $\vec{\sigma}$ are measured, then the term $\vec{p} \cdot \vec{\sigma}$ may occur"[4]; this scalar product is called helicity, it represents the projection of spin onto the momentum and it is the one that characterizes ^{60}Co β-decay experiment. Hence, Yang and Lee's idea was "to measure the angular distribution of the electrons coming from β-decays of oriented nuclei. If θ is the angle between the orientation of the parent nucleus and the momentum of the electron, an asymmetry of distribution between θ and $180° - \theta$ constitutes an unequivocal proof that parity is not conserved in β-decays"[4]. Since the direction of polarization is chosen by the experimenter ($\vec{B}$ along positive z), and so the spin is aligned to the z-axis, then a measurement of θ (polar angle from the z-axis) is also a measurement of the helicity: if θ is small then spin and momentum of e^- have the same orientation, i.e. positive helicity; on the contrary, if θ is large ($\sim 180°$) it means that the momentum points towards negative z, so they have opposite orientation, i.e. negative helicity. In order to assign a value to helicity, quantum mechanics can be used. Since the spin of an electron is $s = 1/2$, then its third component can take only the two values $s_z = +1/2$ and $s_z = -1/2$. That explains also why, once the spins have been aligned along the z-axis, all the electrons will fly with an angle θ either close to 0° or close to 180°, while no electrons will fly along x-axis or y-axis, corresponding to 90°.

A parity transformation makes the e^- in the final state to change helicity, i.e. an e^- that is flying with positive helicity appears to be flying with opposite, negative helicity when looking at its mirror image. Consequently, there is only one possibility such that the mirror image of the experiment is undistinguishable from the actual experiment. The ^{60}Co must emit, in a fixed amount of time, roughly the same number of electrons along the z-axis, i.e. with helicity $s_z = +1/2$, and in the opposite direction, i.e. with helicity $s_z = -1/2$. On the contrary, if more electrons were emitted in one of the two directions, this would imply that at the mirror the preferred direction appears to be the opposite one. This, in turn, would make the 'real' and the mirror experiments perfectly distinguishable, just by measuring which is the helicity of the majority of electrons.

Wu managed to overcome all the complex technical issues, setting up the experiment.

She found that in the decays more electrons are emitted in the direction opposite to nuclear spin, i.e. with helicity $s_z = -1/2$. Therefore, according to the two possible scenarios described above, it can be concluded that weak interactions violate parity. The system is not parity invariant.

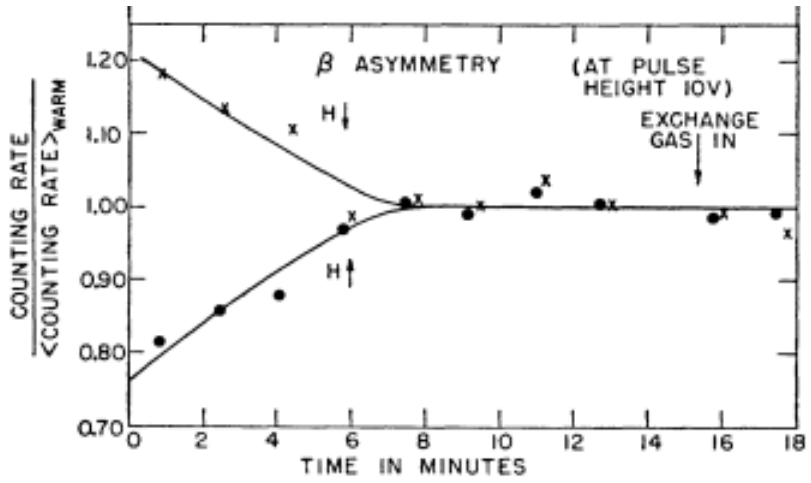

Figure 1.3: Plot of the relative number of electrons emitted opposite to (×) or in the direction of (•) the nuclear spin of ^{60}Co as a function of time. At late times, nuclear polarization is lost due to thermal effects. At early times, the electron is clearly observed to preferentially be emitted opposite to the direction of nuclear spin.[6]

The results obtained in the count experiment are plotted in Fig. 1.3. "The plot shows that actually the asymmetry in the direction of emission of electrons depends on time. The system was cooled to extremely low temperature to ensure the alignment of ^{60}Co nuclei along the magnetic field: thermal excitations had to be small enough to not change orientation of spins. As the system warms up, the thermal excitations eventually completely depolarize the ^{60}Co nuclei, and so after about 6 minutes, a preferred electron's direction is not observed anymore. Before that time, however, the relative number of electrons that are emitted opposite to the spin of the ^{60}Co nuclei is much larger than the number of electrons emitted in the same direction as nuclear spin"[1].

1.5.3 Weinrich's experiment

In Lee and Yang's paper also another test was suggested, which could potentially produce a concrete proof of C violation as well as P violation. It consists of "the decay processes:

$$\pi^+ \to \mu^+ + \nu_\mu, \qquad \mu^+ \to e^+ + \nu_e + \nu_\mu, \tag{1.32}$$

starting from a π meson at rest, one could study the distribution of the angle θ between the μ meson momentum and the electron momentum, the latter being in the center-

of-mass frame of the μ meson. If parity is conserved in neither of the two processes, the distribution will not in general be identical for θ and $180° - \theta$. To understand this, consider first the orientation of the muon spin. If the first process violates parity conservation, the muon would be in general polarized in its direction of motion. In the subsequent decay, the angular distribution problem with respect to θ is therefore closely similar to the angular distribution problem of β-rays from oriented nuclei"[4], which was previously discussed.

This second idea was followed by Garwin, Lederman and Weinrich[7], who realized their experiment shortly after the publication of Wu's results. Looking at the first decay, $\pi^+ \to \mu^+ + \nu_\mu$, the following things must be considered: the pion in the initial state has total momentum $J_i = 0$, thus also the final state must have zero total momentum, $J_f = 0$. Since μ^+ and ν_μ both have spin $s = \frac{1}{2}$, to satisfy the condition $J_f = 0$, the system can have either $L = 0$, $S = 0$ or $L = 1$, $S = 1$; in both cases $J_f = 0$ lies in the range $|L - S| \leq J_f \leq L + S$. However, the small amount of available energy, given by the difference in mass between initial and final states, $m(\pi) - (m(\mu) + m(\nu_\mu)) \approx m(\pi) - m(\mu) \approx 139.5 - 105.5 = 34$ MeV, suggests that the case $L = 1$, $S = 1$ is strongly suppressed. Therefore, the final state must have $L = 0$, $S = 0$, which is possible only if the spins of the two decay products are oppositely aligned. Moreover, considering the reference frame of the decaying pion, the two daughters must have also opposite momentum. These two facts, in turn, imply that the helicity of the muon is the same as that of the neutrino, as it is illustrated in Fig. 1.4.

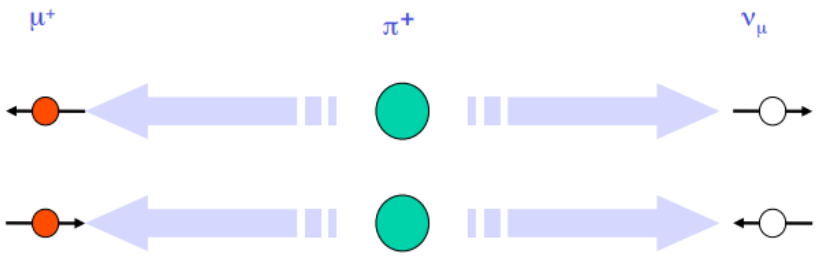

Figure 1.4: Picture illustrating the two possible final configurations of the $\pi^+ \to \mu^+ + \nu_\mu$ decay, in the rest frame of the decaying π^+.

The substantial difference with respect to Wu's experiment is that, in this case, both $\pi^+ \to \mu^+ + \nu_\mu$ and its charge conjugated $\pi^- \to \mu^- + \overline{\nu_\mu}$ can be observed. This is what allows to test also C conservation. It was measured that the majority of μ^+ produced in the decays has negative helicity, while the majority of μ^- has positive helicity. The experimental evidence of a preferred helicity associated to muons implies that P symmetry is violated (analogously to Wu's experiment). Moreover, the fact that the opposite helicity is preferred by anti-muons, proves in turn that also C symmetry is violated.

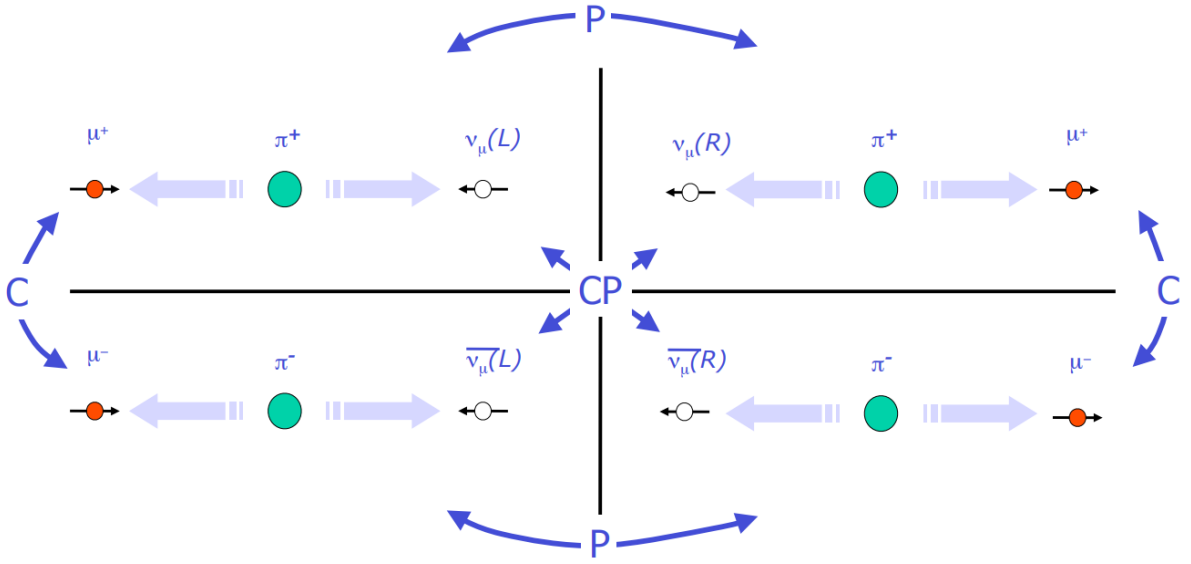

Figure 1.5: Picture illustrating the four possible configurations of the two $\pi^{\pm} \to \mu^{\pm} + \nu_{\mu}$ decays. Their connections via parity, charge conjugation and the combination of the two transformations are also indicated.

One can understand what is obtained after a CP transformation starting for example from $\pi^+ \to \mu^+ + \nu_\mu$ decays as they are observed, i.e. the majority of anti-muons has negative helicity: their spin is oriented inwards with respect to the initial pion position and their momentum is oriented outwards. Consider one of these anti-muons, whose trajectory can be fixed leftwards and consequently its spin is oriented rightward. After a parity transformation the momentum is flipped rightwards as well, hence the anti-muon appears to have positive helicity. Secondly, charge conjugation transforms this positively charged anti-muon into a negatively charged muon, without acting neither on vectors nor on pseudo-vectors. Therefore, the final result of the combination of the two transformations is a muon with positive helicity. This is shown in Fig. 1.5. To sum up, $\pi^+ \to \mu^+ + \nu_\mu$ decays that undergo a CP transformation look identical to the observable $\pi^- \to \mu^- + \overline{\nu_\mu}$ decays: in both cases the majority of muons is measured to have positive helicity. Thus, CP symmetry is conserved.

In this system, the violation of C symmetry, beyond P-symmetry violation, ensures that CP symmetry is restored. As a consequence, T symmetry must be preserved, thanks to CPT theorem. On the contrary, T symmetry can be flagrantly broken in classical systems, where a large number of particles interact, that is also the reason why the concept of entropy was introduced. So, at first it was not clear whether T symmetry had to preserved or not at fundamental level. This directly reflects also on CP symmetry.

1.6 CP violation

1.6.1 Neutral kaon system

Strong interactions produce the neutral kaons $K^0(d\bar{s})$ and its antiparticle $\overline{K}^0(s\bar{d})$. They have definite strangeness and can be identified as two eigenstates belonging to the strong basis, this because strong interactions preserve quarks' flavour and they present different strangeness, respectively +1 and -1. Moreover, they are in the fundamental state, i.e. they are stable with respect to strong interactions, so they can decay only via weak interactions. However, the two neutral kaons can mix together under weak interactions, i.e. a K^0 can turn into a $\overline{K}^0$ and vice versa. The process goes under the name of strangeness oscillations and it is characterized by $|\Delta S = 2|$; the box diagrams are illustrated in Fig. 1.6 and Fig. 1.7:

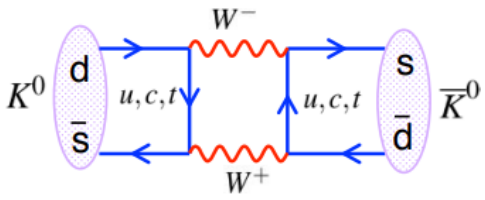

Figure 1.6: Box diagram of $K^0 \to \overline{K}^0$. It can be read as follows; the anti-quark strange emits a W^+ boson and turns into an anti-quark up which then annihilates with the down quark producing a W^- boson. In the meanwhile the W^+ boson (first emitted) creates a couple up quark, anti-quark down; the former absorbs the W^- boson becoming so a strange quark.

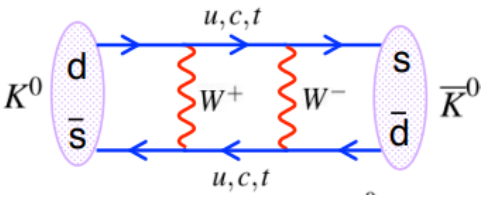

Figure 1.7: Box diagram of $K^0 \to \overline{K}^0$. It can be read as follows; the down quark turns into an up quark absorbing a W^+ boson and finally into a strange quark absorbing a W-boson; the two bosons come from the anti-quark strange, that turns into an anti-quark up emitting a W+ boson and finally into a anti-quark down emitting a W^- boson.

Strangeness oscillations imply that K^0 and $\overline{K}^0$ are not orthogonal under weak interactions, therefore strong eigenstates $|K^0\rangle$ and $|\overline{K}^0\rangle$ individually do not represent also weak eigenstates.

At the beginnings weak interactions were thought to preserve CP symmetry, as suggested by Wu's experiment, and this led to identify weak eigenstates with CP eigenstates. It can be demonstrated that neither $|K^0\rangle$ nor $|\overline{K}^0\rangle$ are eigenstates of CP symmetry. In fact, both $|K^0\rangle$ and $|\overline{K}^0\rangle$ have $J^P = 0^-$, therefore one can apply the parity operator obtaining

$$\hat{P}|K^0\rangle = -|K^0\rangle \quad \text{and similarly} \quad \hat{P}|\overline{K}^0\rangle = -|\overline{K}^0\rangle. \tag{1.33}$$

On the other hand, the charge conjugation operator turns a particle into its anti-particle and vice versa,

$$\hat{C}|K^0\rangle = |\overline{K}^0\rangle \quad \text{and similarly} \quad \hat{C}|\overline{K}^0\rangle = |K^0\rangle. \tag{1.34}$$

Then, applying both the operators in sequence one gets

$$\hat{C}\hat{P}|K^0\rangle = -|\overline{K}^0\rangle \quad \text{and similarly} \quad \hat{C}\hat{P}|\overline{K}^0\rangle = -|K^0\rangle. \tag{1.35}$$

The two equations do not return the initial state, as so $|K^0\rangle$ and $|\overline{K}^0\rangle$ are not CP eigenstates, as claimed. Despite that, a normalized linear combination of the two of them can be made, getting

$$|K_1\rangle = \frac{1}{\sqrt{2}}(|K^0\rangle - |\overline{K}^0\rangle) \quad \text{and} \quad |K_2\rangle = \frac{1}{\sqrt{2}}(|K^0\rangle + |\overline{K}^0\rangle), \tag{1.36}$$

which are manifestly independent and further both of them are CP eigenstates. In fact:

$$\hat{C}\hat{P}|K_1\rangle = \hat{C}\hat{P}(|K^0\rangle - |\overline{K}^0\rangle)\frac{1}{\sqrt{2}} = (-|\overline{K}^0\rangle + |K^0\rangle)\frac{1}{\sqrt{2}} = |K_1\rangle, \tag{1.37}$$

and analogously

$$\hat{C}\hat{P}|K_2\rangle = \hat{C}\hat{P}(|K^0\rangle + |\overline{K}^0\rangle)\frac{1}{\sqrt{2}} = (-|\overline{K}^0\rangle - |K^0\rangle)\frac{1}{\sqrt{2}} = -|K_2\rangle, \tag{1.38}$$

with eigenvalues +1 and -1 respectively.

Neutral kaons can decay weakly (without conserving flavours) to pions, the lightest mesons, in either two or three of them. This because the kaon mass is approximately 498 MeV, that is greater than three times the pion mass, which is approximately 140 MeV (cannot decay in four or even more pions because this would violate the energy conservation). In order to preserve at least the electrical charge, the two-pions final states can be either $K^0 \to \pi^0 + \pi^0$ or $K^0 \to \pi^+ + \pi^-$. In both cases the final states are CP-symmetry eigenstates with positive eigenvalue: $\hat{C}\hat{P}|\pi^0\pi^0\rangle = +1$ and likewise $\hat{C}\hat{P}|\pi^+\pi^-\rangle = +1$. This means that the decay of a neutral kaon in two pions has a well-defined positive CP symmetry. In the hypothesis that weak interactions conserve CP, it can be concluded that only the CP eigenstate $|K_1\rangle$, which also has CP symmetry +1, can decay to two pions.

The decays into three pions can be of two types as well, $K^0 \to \pi^0 + \pi^0 + \pi^0$ and $K^0 \to \pi^+ + \pi^- + \pi^0$. In both cases the final states are CP-symmetry eigenstates with negative eigenvalue: $\hat{C}\hat{P}|\pi^0\pi^0\pi^0\rangle = -1$ and likewise $\hat{C}\hat{P}|\pi^+\pi^-\pi^0\rangle = -1$. This shows that also the decay of a neutral kaon into three pions has a well-defined negative CP symmetry. In the hypothesis that weak interactions conserve CP symmetry it can be concluded that only the CP eigenstate $|K_2\rangle$, which also has CP symmetry -1, can decay to three pions.

Experimentally, two physical states are observed to exist: the first has a short lifetime, it's called K-short (indicated by K_S) and often decays to two pions; the second has a relatively longer lifetime, therefore called K-long (indicated by K_L) and often decays to three pions. More precisely, the lifetime of K-long is three orders of magnitude longer than that of K-short, approximately $5.1 \times 10^{-8}s$ against $8.9 \times 10^{-11}s$. The hypothesis that weak interactions conserve CP symmetry suggests to identify $|K_S\rangle$ with $|K_1\rangle$, the one CP eigenstate that is allowed to decay in two pions and similarly $|K_L\rangle$ with $|K_2\rangle$, which according to CP conservation cannot decay in two but three pions. "Unlike K^0 and $\overline{K^0}$, distinguished by their mode of production, K_S and K_L are distinguished by their mode of decay"[8].

The large gap between the two lifetimes can be explained calculating the available energy for the decay in each of the two cases, which corresponds to the difference between the initial state mass and the final state mass, composed of either two or three pions:

$$m(K^0) - 2m(\pi) \approx 220\ \text{MeV},$$
$$m(K^0) - 3m(\pi) \approx 80\ \text{MeV};$$

the available energy for the kinematic of the products in the two pions decay is greater and so the kinematic parameters can assume a wider range of values, and therefore it has more possible ways of happening. This results in the two-pions decay to be more likely and thus to take place at a higher rate.

In 1964, Christenson, Fitch, Cronin and Turlay looked for the decay products of a beam of K^0 at long distance from its origin[**cronin**]. In order to understand how it behaves during propagation, $|K^0\rangle$ can be expanded in the weak basis, which is made by CP eigenstates according to the previous hypothesis. This can be easily obtained inverting the expansions of CP eigenstates $|K_1\rangle$ and $|K_2\rangle$ in the strong basis and the result is:

$$\psi(0) = |K^0(0)\rangle = \frac{1}{\sqrt{2}}(|K_S(0)\rangle + |K_L(0)\rangle). \tag{1.39}$$

The time evolution of the wave function that describes an unstable particle of mass m and lifetime $\tau = \frac{1}{\Gamma}$ in the centre of mass frame, where $E = m$, can be written as:

$$\psi(t) = \psi(0)e^{-imt-\frac{\Gamma}{2}t}, \tag{1.40}$$

which correctly gives $|\psi(t)|^2 = |\psi(0)|^2 e^{-\Gamma t} = |\psi(0)|^2 e^{-\frac{t}{\tau}}$. K_S and K_L have different lifetimes and possibly different masses, so their time evolution can be expressed as follows

$$\psi(t) = \frac{1}{\sqrt{2}}(|K_S(0)\rangle e^{-im_S t - \frac{\Gamma_S}{2}t} + |K_L(0)\rangle e^{-im_L t - \frac{\Gamma_L}{2}t}). \tag{1.41}$$

An analytical expression can be obtained for the intensity of K_0, that is proportional to the number of K_0, as time flows, using Dirac formalism

$$I(K^0) = |\langle K^0|\psi(t)\rangle|^2 \tag{1.42}$$

using that $|K_S\rangle$ and $|K_L\rangle$ can be expanded in the strong basis as $|K_1\rangle = \frac{1}{\sqrt{2}}(|K^0\rangle - |\overline{K}^0\rangle)$ and $|K_2\rangle = \frac{1}{\sqrt{2}}(|K^0\rangle + |\overline{K}^0\rangle)$,

$$I(K^0) = |\langle K^0|K^0\rangle|^2 \left|\frac{1}{\sqrt{2}}\left(\frac{1}{\sqrt{2}}e^{-im_S t - \frac{\Gamma_S}{2}t} + \frac{1}{\sqrt{2}}e^{-im_L t - \frac{\Gamma_L}{2}t}\right)\right|^2, \tag{1.43}$$

$$I(K^0) = \frac{1}{4}\left(e^{-\Gamma_S t} + e^{-\Gamma_L t} + e^{-i(m_S - m_L)t - \left(\frac{\Gamma_S}{2} + \frac{\Gamma_L}{2}\right)t} + e^{+i(m_S - m_L)t - \left(\frac{\Gamma_s}{2} + \frac{\Gamma_L}{2}\right)t}\right), \tag{1.44}$$

which can be written using $\Delta m \equiv m_L - m_S$ and that $\cos(x) = \frac{e^{ix} + e^{-ix}}{2}$,

$$I(K^0) = \frac{1}{4}\left(e^{-\Gamma_S t} + e^{-\Gamma_L t} + 2e^{-\left(\frac{\Gamma_S}{2} + \frac{\Gamma_L}{2}\right)t}\cos(\Delta m t)\right) \tag{1.45}$$

An empirical measurement of $I(K^0)$ can be made to obtain the frequency of oscillation, which in turn depends on Δm.

$|K^0\rangle$ is a combination of the short-lived component $|K_S\rangle$ and the long-lived component $|K_L\rangle$. For this reason, it can decay in both two or three pions, but two-pions decays are dominant in the region near the beam origin, while as distance increases three-pions decays become prevalent; going even further there will be a threshold that once crossed will give almost certainty of having a pure K_L beam; this is resumed schematically in Fig. 1.8.

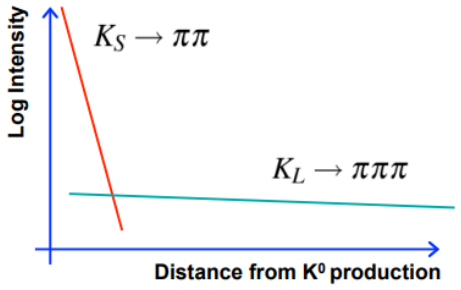

Figure 1.8: Qualitative plot of the intensity of the two decays $K_S \to \pi + \pi$ and $K_L \to \pi + \pi + \pi$ as a function of distance from the origin of the pure K^0 beam.

In practice, K^0 with a momentum $p \approx 1$ GeV/c were obtained bombarding a Berillium target with a proton beam of energy $E = 30$ GeV. The component with short lifetime K_S had a decay length of the order of 10 cm, so the K^0 had to travel a 15 m long vacuum tube before reaching the detectors, thus becoming a pure K_L beam once there. Anyhow, the scientists observed 45 decays into a pair of oppositely charged pions in a sample of 22700 kaon decays, almost 1 every 500. This kind of decay arrives at a final state that has CP symmetry opposite with respect to the initial CP symmetry of K_L and thus proves that CP is not preserved exactly by weak interactions, but rather it is slightly violated.

Exploiting the fact that the products of decay are identical particles (pions), a two-body decay could be distinguished from a three-body decay measuring the angle θ from the forward direction of the vector sum of the two momenta of π^+ and π^-. In fact, due to the conservation of momentum, if the products of the decay are actually only those two, then the sum of the two momentum vectors must be parallel to the incident beam direction, i.e. $\theta = 0$, whereas this is not true in general if the bodies are three. In this latter case, where the neutral pion π^0 is not detected, the vectorial sum of the momenta of the two charged pions can take any direction, following a continuous distribution, since the constraint is fulfilled when also the third momentum vector is taken into consideration. The results of the measurement of the angle θ are shown in Fig. 1.9

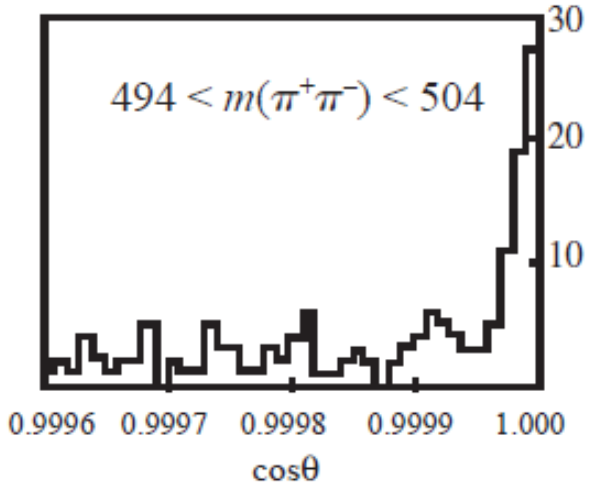

Figure 1.9: Distribution of cosθ around K mass. Originally obtained in 1964[**cronin**]. The peak around cos$\theta = 1$ indicates decays into two charged pions.

Accepting experimental evidence that $BR(K_L \to \pi^+ + \pi^-) = (2.090 \pm 0.025) \cdot 10^{-3}$, the previous hypothesis of CP symmetry must be rejected. CP violation has various sources, which can be classified.

1.6.2 Sources of CP violation

- CP violation in the mixing: the hypothesis is that, given some neutral meson M, the physical eigenstates M-short and M-long (or equivalently M-light and M-heavy) do not correspond precisely to the CP eigenstates. In particular, in the neutral kaon system this means that the mass eigenstate $|K_L\rangle$ is a linear superposition of the CP eigenstates $|K_1\rangle$ and $|K_2\rangle$; as a consequence, the measured decay channel $K_L \to \pi + \pi$ becomes actually possible, thanks to the $|K_1\rangle$ component of $|K_L\rangle$. One could write

$$|K_S\rangle = \frac{1}{\sqrt{1+|\epsilon|^2}}\left(|K_1\rangle + \epsilon|K_2\rangle\right) \quad \text{and similarly} \quad |K_L\rangle = \frac{1}{\sqrt{1+|\epsilon|^2}}\left(|K_2\rangle + \epsilon|K_1\rangle\right) \tag{1.46}$$

where the complex parameter ϵ has been added, satisfying $|\epsilon|^2 \ll 1$. It is in fact the small quantity that somehow measures the amount of CP violation induced by the mixing of states. The physical states $|K_S\rangle$ and $|K_L\rangle$ written in this way are not CP eigenstates anymore and they are not even orthogonal, so they can share the same decay channels. In Dirac formalism, the extent to which the two physical eigenstates are not orthogonal is given by $\langle K_S|K_L\rangle$:

$$\begin{aligned}
\langle K_S|K_L\rangle =& \frac{1}{1+|\epsilon|^2}\left(\langle K_1| + \epsilon^*\langle K_2|\right)\left(|K_2\rangle + \epsilon|K_1\rangle\right) && (1.47)\\
=& \frac{1}{1+|\epsilon|^2}\left(\langle K_1|K_2\rangle + \epsilon\langle K_1|K_1\rangle + \epsilon^*\langle K_2|K_2\rangle + \epsilon^*\epsilon\langle K_2|K_2\rangle\right) && (1.48)\\
=& \frac{1}{|\epsilon|^2}\left(\epsilon + \epsilon^*\right) && (1.49)\\
=& \frac{2Re(\epsilon)}{1+|\epsilon|^2}, && (1.50)
\end{aligned}$$

where the orthogonality of CP eigenstates $|K_1\rangle$ and $|K_2\rangle$ has been used. The two physical eigenstates $|K_L\rangle$, $|K_S\rangle$ can be expressed also in terms of the strangeness eigenstates, replacing the CP eigenstates $|K_1\rangle$, $|K_2\rangle$ with their expansions in the strong basis, made by $|K^0\rangle$ and $|\overline{K}^0\rangle$.

$$|K_L\rangle = \frac{1}{\sqrt{1+|\epsilon|^2}}\left[\frac{1}{\sqrt{2}}\left(|K^0\rangle + |\overline{K}^0\rangle\right) + \epsilon\left(\frac{1}{\sqrt{2}}\left(|K^0\rangle - |\overline{K}^0\rangle\right)\right)\right], \tag{1.51}$$

$$|K_L\rangle = \frac{1}{\sqrt{2}}\frac{1}{\sqrt{1+|\epsilon|^2}}\left[\left(1+\epsilon\right)|K^0\rangle + \left(1-\epsilon\right)|\overline{K}^0\rangle\right], \tag{1.52}$$

while

$$|K_S\rangle = \frac{1}{\sqrt{1+|\epsilon|^2}}\left[\frac{1}{\sqrt{2}}\left(|K^0\rangle - |\overline{K}^0\rangle\right) + \epsilon\left(\frac{1}{\sqrt{2}}\left(|K^0\rangle + |\overline{K}^0\rangle\right)\right)\right], \tag{1.53}$$

$$|K_S\rangle = \frac{1}{\sqrt{2}} \frac{1}{\sqrt{1+|\epsilon|^2}} \left[(1+\epsilon)\,|K^0\rangle - (1-\epsilon)\,|\overline{K}^0\rangle \right]. \tag{1.54}$$

The two expressions can also be rewritten as $|K_L\rangle = p|K^0\rangle + q|\overline{K}^0\rangle$ and $|K_S\rangle = p|K^0\rangle - q|\overline{K}^0\rangle$, where p, q are complex factors such that $|p|^2 + |q|^2 = 1$; thus, the condition for CP violation in the mixing can be expressed also as $|\frac{p}{q}| \neq 1$.

Pure CP violation in the mixing can be observed for neutral kaon system, in the semileptonic decay modes of K_L. Consider the decays

$$K_L \to e^+ + \nu_e + \pi^- \quad \text{and} \quad K_L \to e^- + \overline{\nu_e} + \pi^+, \tag{1.55}$$

where the two final states are connected via CP transformation and can be easily distinguished in a detector by the sign of the electron's charge. Each of the two is "a flavour-specific decay, i.e. a decay into a final state which can only be reached from an initial K^0 (or $\overline{K^0}$) but not from both"; specifically, "the decay into a positively charged lepton can come only from the K^0 component of the beam, and decay into a negative lepton only from the $\overline{K^0}$ component"[8]. Last but not least, in the SM the two decay modes have the same transition amplitudes (each of them has one contribute only), i.e. $|A(K^0 \to e^+ + \nu_e + \pi^-)| = |A(\overline{K^0} \to e^- + \overline{\nu_e} + \pi^+)|$, beside $|A(K^0 \to e^- + \overline{\nu_e} + \pi^+)| = |A(\overline{K^0} \to e^+ + \nu_e + \pi^-)| = 0$. If CP symmetry were conserved, then $|K_L\rangle = |K_2\rangle = \frac{1}{\sqrt{2}}(|K^0\rangle + |\overline{K}^0\rangle)$, where $|K^0\rangle$ and $|\overline{K}^0\rangle$ are equiprobable, hence one would expect the same decay rates for both final states, i.e. an equal number of positron and electron produced. The following observable can be defined,

$$\Delta = \frac{\Gamma(K_L \to e^+ + \nu_e + \pi^-) - \Gamma(K_L \to e^- + \overline{\nu_e} + \pi^+)}{\Gamma(K_L \to e^+ + \nu_e + \pi^-) + \Gamma(K_L \to e^- + \overline{\nu_e} + \pi^+)}. \tag{1.56}$$

The measurement of the asymmetry was done, and the results are reported in Fig. 1.10.

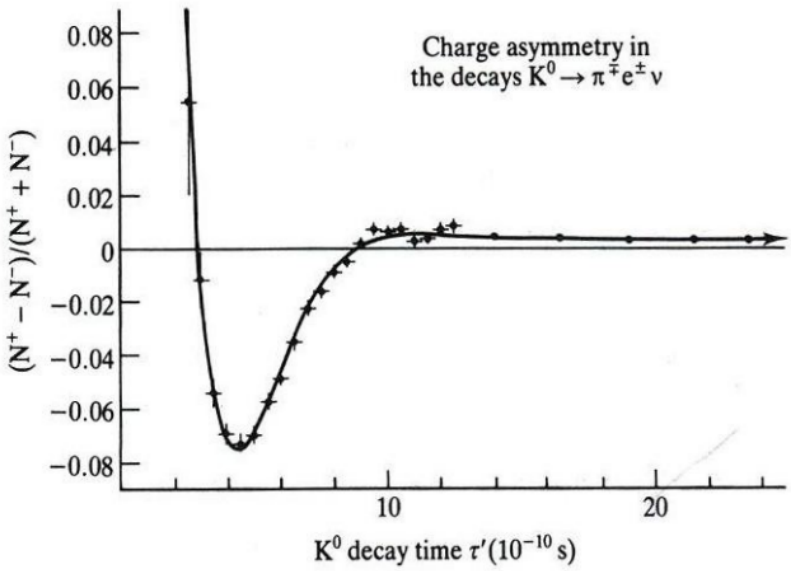

Figure 1.10: Plot of the charge asymmetry in the semileptonic decays $K^0 \to e^+ + \nu_e + \pi^-$ and $\overline{K^0} \to e^- + \overline{\nu_e} + \pi^+$ as a function time.[3]

$|K_L\rangle$, which is the only mass eigenstate left at long distance from the origin of a K^0 beam (corresponding to many K_S-lifetimes), shows a preference for the production of positrons, i.e. $\Delta > 0$.

This small charge asymmetry represented the first proof that matter and antimatter are not treated on equal footing by weak interactions, at least when CP violation is involved. Thanks to it, a first definition can be given to distinguish between positive and negative electric charges, calling negative charge that of the lepton emitted less often in the decays of K_L.

Going back to calculations, given the existence of an asymmetry, $|K_L\rangle$ must be expressed as

$$|K_L\rangle = \frac{1}{\sqrt{2}} \frac{1}{\sqrt{1+|\epsilon|^2}} \left[(1+\epsilon)\,|K^0\rangle + (1-\epsilon)\,|\overline{K}^0\rangle \right]; \tag{1.57}$$

recalling that positrons come only from K^0 while electrons only from $\overline{K^0}$, the asymmetry can be rewritten as

$$\Delta = \frac{|1+\epsilon|^2 - |1-\epsilon|^2}{|1+\epsilon|^2 + |1-\epsilon|^2}, \tag{1.58}$$

and after some algebraic manipulations, it becomes

$$\Delta = \frac{2Re(\epsilon)}{1+|\epsilon|^2}. \tag{1.59}$$

Thus, the empirical measurement of the asymmetry Δ returns the value of the real part of ϵ, which corresponds to the amount of non orthogonality in the mixing of $|K_S\rangle$ and $|K_L\rangle$.

From a theoretical perspective, the Hamiltonian which includes weak interactions together with strong and electromagnetic ones is not diagonal anymore and so its eigenstates, the physical eigenstates, are no longer $|K^0\rangle$ and $|\overline{K^0}\rangle$, due to their mixing via weak interactions. Furthermore, there exist different ways to transit from K^0 to $\overline{K^0}$, via box diagrams (view Fig. 1.6 and Fig. 1.7). As a result, the two probabilities of oscillation, proportional to the squared modulus of the corresponding transition amplitude, are different, $P(K^0 \to \overline{K^0}) \neq P(\overline{K^0} \to K^0)$. Hence, the two mass eigenstates, which can be obtained diagonalizing the Hamiltonian, are found to be mixture in unequal proportions of the two flavour eigenstates. In light of this, CP violation in the mixing can be thought of as an intrinsic property of the physical eigenstates.

Generically, it is measured by

$$\Delta = \frac{\Gamma\left(\overline{M^0}(t) \to l^+X^-\right) - \Gamma\left(M^0(t) \to l^-X^+\right)}{\Gamma\left(\overline{M^0}(t) \to l^+X^-\right) + \Gamma\left(M^0(t) \to l^-X^+\right)}, \tag{1.60}$$

where M represents some meson, $l^\pm$ is typically an electron or a muon, and X groups all the other decay products.

- CP violation in the decay: "If the flavour of the decaying meson M is known, any observed difference between the decay rate $\Gamma(M \to f)$ and its CP conjugate rate $\Gamma(\overline{M} \to \overline{f})$ would indicate that CP is directly violated in the decay amplitude"[9].

  In the theoretical framework, it results from interference between various terms (at least two) contributing to the same decay amplitude $A(M \to f)$, i.e. when $A(M \to f) = \sum_i A_i e^{i(\delta_i+\phi_i)}$, where ϕ_i are the weak phases and δ_i are the strong phases. This because the decay rate $\Gamma(M \to f)$ depends on the squared modulus of the transition amplitude $A(M \to f)$; hence, if this latter is composed of two distinct elementary decay amplitudes, two complex terms, when the squared modulus is taken, a third term pops out. The crucial aspect is that once the decay rate of the CP-transformed decay is considered, $\Gamma(\overline{M} \to \overline{f})$, the "interference" term is different, because the weak phases ϕ_i of the two elementary decay amplitudes change sign while their strong phases δ_i do not. To sum up, CP violation in decay amplitude occurs if $\frac{|A(\overline{M}\to\overline{f})|}{|A(M\to f)|} = \frac{|\sum_i A_i e^{i(\delta_i-\phi_i)}|}{|\sum_i A_i e^{i(\delta_i+\phi_i)}|} \neq 1$.

  Pure CP violation in the decay can be studied in charged-mesons decays, such as $K^\pm \to \pi^\pm + \pi^0$, where the charge of the final products clearly identifies the flavour of the decaying meson. Note that K^+ and K^- cannot oscillate like K^0 and $\overline{K^0}$

do, because of conserved of electric charge, so a difference in the decaying rate can come only from a difference in the amplitudes. For generic charged mesons $M^{\pm}$ that decay respectively in the final states $f^{\pm}$, this is the only possibility of CP violation and it is measured defining the observable asymmetry

$$\Delta = \frac{\Gamma(M^+ \to f^+) - \Gamma(M^- \to f^-)}{\Gamma(M^+ \to f^+) + \Gamma(M^- \to f^-)}. \tag{1.61}$$

Back to the neutral kaon system, CP violation in the decay arises when $K^0, \overline{K^0} \to \pi + \pi$ ($\Delta S = 1$) since different types of diagram give their contribute, beside, the system of two pions can be found with isospin $I = 0$ or $I = 2$; all this results in interfering amplitudes with different weak phases and strong phases.

- CP violation in the interference between a decay without mixing and a decay with mixing: it is possible when both neutral mesons M^0 and $\overline{M^0}$ share the same final state, e.g. a CP eigenstate f_{CP}", so that $f_{CP} = \overline{f_{CP}}$. It follows that there will be two amplitudes contributing to the transition amplitude from the initial state M^0 to a final state f; they are $A(M^0 \to f)$ and $A(M^0 \to \overline{M^0} \to f_{CP})$, thus potentially interfering. This source of CP violation can be measured as

$$\Delta = \frac{\Gamma(M^0(t) \to f_{CP}) - \Gamma(\overline{M^0}(t) \to f_{CP})}{\Gamma(M^0(t) \to f_{CP}) + \Gamma(\overline{M^0}(t) \to f_{CP})}. \tag{1.62}$$

Note that this kind of CP violation can be present even if neither CP violation in the mixing nor in the decay are present. This source of CP violation, when singled out, is due to the fact that M^0 and $\overline{M^0}$ oscillate (non necessarily producing CP violation in mixing); for this reason it is also called mixing-induced CP violation. In the neutral kaon system the final states $|\pi^+\pi^-\rangle$ and $|\pi^0\pi^0\rangle$ are both CP eigenstates, common to $|K^0\rangle$ and $|\overline{K}^0\rangle$, so mixing-induced CP violation may be present.

A different classification distinguishes between indirect and direct CP violation. It can be applied to the case of neutral kaon system. Indirect CP violation accounts only for those CP violations due to strangness oscillations, transitions with $|\Delta S = 2|$; clearly CP violation in the mixing belongs to this class. On the other hand, direct CP violations are caused by transitions with $\Delta S = 1$, hence CP violation in the decay is part of this class. "The importance of distinguishing among these two types of CP violation lies in the fact that the former only appears in the mixing of flavoured mesons and anti-mesons, which is observable as an intrinsic property of the physical meson states, induced by their mutual virtual interactions, while the latter is a general property of the flavour-changing weak interactions"[10]. Note that indirect CP violation can happen only in neutral meson systems and, at first, it was thought to be the only admissible cause of CP violation; in fact, this classification was made earlier than the other one. CP violation in the

interference between a decay without mixing and a decay with mixing is induced by strangeness oscillations and hence can be thought of as indirect CP violation; however, when the final state is common to M^0 and $\overline{M^0}$, in general, all three types of CP violation can occur and so indirect and direct CP violation may coexist. This is exactly the case of $K^0, \overline{K^0} \to \pi + \pi$ decays. In order to quantify the amount of direct and indirect CP violation, one can define

$$\eta_{+-} \equiv \frac{A(K_L \to \pi^+ + \pi^-)}{A(K_S \to \pi^+ + \pi^-)} \quad \text{and} \quad \eta_{00} \equiv \frac{A(K_L \to \pi^0 + \pi^0)}{A(K_S \to \pi^0 + \pi^0)}. \tag{1.63}$$

They are amplitude ratios that take into consideration the two physical states. If only indirect CP violation were present, the two ratios could be written as

$$\eta_{+-} = \frac{\langle \pi^+\pi^-|H|\epsilon K_1\rangle}{\langle \pi^+\pi^-|H|K_1\rangle} \quad \text{and} \quad \eta_{00} = \frac{\langle \pi^0\pi^0|H|\epsilon K_1\rangle}{\langle \pi^0\pi^0|H|K_1\rangle}. \tag{1.64}$$

Thus, it is clear that given this hypothesis the two ratios are supposed to return the same value, precisely $\eta_{+-} = \eta_{00} = \epsilon$. Therefore, a difference from the unit of the ratio between η_{+-} and η_{00}, would imply that the amount of CP violation depends on the decay and so it must be a signal of direct CP violation. Indeed, taking into account direct CP violation as well, i.e. the differences between the amplitudes, $A(K^0 \to \pi^+ + \pi^-) \neq A(\overline{K^0} \to \pi^+ + \pi^-)$ and $A(K^0 \to \pi^0 + \pi^0) \neq A(\overline{K^0} \to \pi^0 + \pi^0)$, it can be calculated that

$$\eta_{+-} \approx \epsilon + \epsilon' \quad \text{and} \quad \eta_{00} \approx \epsilon - 2\epsilon', \tag{1.65}$$

where ϵ' is a complex factor such that $\epsilon' \neq 0$ would reveal direct CP violation.

1.7 CKM matrix

After GIM prediction, Cabibbo matrix can be rewritten in a more generic form as

$$\begin{pmatrix} d' \\ s' \end{pmatrix} = \begin{pmatrix} V_{ud} & V_{us} \\ V_{cd} & V_{cs} \end{pmatrix} \begin{pmatrix} d \\ s \end{pmatrix}. \tag{1.66}$$

It is a real matrix, whose elements depend only on one real parameter, θ_C. The matrix is orthogonal, and orthogonal matrices are also unitary. In fact, a matrix V for which $V^T V = 1$ is called orthogonal, but since the matrix is also real $V^* = V$, and likewise $V^{*T} = V^T$. Hence substituting this in the definition of orthogonal matrix, one gets $V^{*T}V = 1$ that is actually the definition of a unitary matrix. The unitarity condition is fundamental in quantum physics because it ensures the conservation of probability.

In 1973 Kobayashi and Maskawa generalised the 2×2 unitary Cabibbo matrix to a 3×3 unitary matrix, the so called CKM matrix. The quark mixing transformation to

obtain the weak eigenstates from mass eigenstates thus becomes

$$\begin{pmatrix} d' \\ s' \\ b' \end{pmatrix} = \begin{pmatrix} V_{ud} & V_{us} & V_{ub} \\ V_{cd} & V_{cs} & V_{cb} \\ V_{td} & V_{ts} & V_{tb} \end{pmatrix} \begin{pmatrix} d \\ s \\ b \end{pmatrix}. \tag{1.67}$$

The reason why they did so is that Cabibbo matrix does not allow for CP violation while CKM matrix does, but this will be clearer soon. A 3×3 complex matrix is described by $3^2 = 9$ complex elements, i.e. $2 \cdot 9 = 18$ real elements. However, unitarity condition $VV^+ = 1$

$$\begin{pmatrix} V_{ud} & V_{us} & V_{ub} \\ V_{cd} & V_{cs} & V_{cb} \\ V_{td} & V_{ts} & V_{tb} \end{pmatrix} \begin{pmatrix} V_{ud}^* & V_{cd}^* & V_{td}^* \\ V_{us}^* & V_{cs}^* & V_{ts}^* \\ V_{ub}^* & V_{cb}^* & V_{tb}^* \end{pmatrix} = \begin{pmatrix} 1 & 0 & 0 \\ 0 & 1 & 0 \\ 0 & 0 & 1 \end{pmatrix}, \tag{1.68}$$

provides six independent conditions, the row-column products that return the elements on the main diagonal and on the upper triangle of the identity matrix:

$$V_{ud}V_{ud}^* + V_{us}V_{us}^* + V_{ub}V_{ub}^* = 1, \tag{1.69}$$
$$V_{cd}V_{cd}^* + V_{cs}V_{cs}^* + V_{cb}V_{cb}^* = 1, \tag{1.70}$$
$$V_{td}V_{td}^* + V_{ts}V_{ts}^* + V_{tb}V_{tb}^* = 1, \tag{1.71}$$
$$V_{ud}V_{cd}^* + V_{us}V_{cs}^* + V_{ub}V_{cb}^* = 0, \tag{1.72}$$
$$V_{ud}V_{td}^* + V_{us}V_{ts}^* + V_{ub}V_{tb}^* = 0, \tag{1.73}$$
$$V_{cd}V_{td}^* + V_{cs}V_{ts}^* + V_{cb}V_{tb}^* = 0. \tag{1.74}$$

Note that the first three relations ensure weak universality, i.e. the universality of the coupling constant, since they force the sum of the squared moduli of the couplings of u with the down-like quarks d, s, b to be 1, likewise for c and t. Other three independent conditions are obtained writing down $V^+V = 1$ and taking again the three row-column products that return the elements on the upper triangle of the identity matrix.

$$V_{ud}^*V_{us} + V_{cd}^*V_{cs} + V_{td}^*V_{ts} = 0, \tag{1.75}$$
$$V_{ud}^*V_{ub} + V_{cd}^*V_{cb} + V_{td}^*V_{tb} = 0, \tag{1.76}$$
$$V_{us}^*V_{ub} + V_{cs}^*V_{cb} + V_{ts}^*V_{tb} = 0. \tag{1.77}$$

So, $18 - 9 = 9$ real parameters are left; three of them are the angles that define a generic rotation in three dimensions, while the remaining six must be complex phases. Moreover, not all six of them are significant, in fact, the following couple of transformations can be applied for each of the six quarks, e.g.

$$d \to e^{i\theta_d} d \quad \text{and} \quad V_{id} \to e^{-i\theta_d} V_{id} \quad \text{where} \quad i = u, c, t; \tag{1.78}$$

if such a transformation is done for all six quarks, then for example $V_{ud} \to e^{-i(\theta_d - \theta_u)} V_{ud}$; thus the matrix is invariant only if $\theta_d = \theta_u$ and analogously for all couples of angles. This

gives five more constraints on the phases, i.e. only one can be arbitrarily chosen. It is this phase factor $e^{i\delta}$, which for anti-particles becomes $e^{-i\delta}$, that can cause CP violation, under certain circumstances, and thus also T violation.

The CKM elements are fundamental parameters, i.e. they are used in the Standard Model but cannot be predicted theoretically, so their measurements should be as precise as possible. The present-day accepted measurements of the moduli of the elements of the CKM matrix are

$$\begin{pmatrix} |V_{ud}| & |V_{us}| & |V_{ub}| \\ |V_{cd}| & |V_{cs}| & |V_{cb}| \\ |V_{td}| & |V_{ts}| & |V_{tb}| \end{pmatrix} = \begin{pmatrix} 0.97435 \pm 0.00016 & 0.22501 \pm 0.00068 & 0.003732 \pm 0.000090 \\ 0.22487 \pm 0.00068 & 0.97349 \pm 0.00016 & 0.04183 \pm 0.00079 \\ 0.00858 \pm 0.00019 & 0.04111 \pm 0.00077 & 0.999118 \pm 0.000034 \end{pmatrix} \tag{1.79}$$

which show that the mixing of flavors happens only in small proportions, since the elements on the main diagonal are much larger. This new model proposed by Kobayashi and Maskawa successfully explains the measured asymmetries, and the existence of the new doublet of quarks, top and bottom, that they had to introduce was later experimentally confirmed.

These were some of the steps that led towards the creation of the SM.

Chapter 2

The LHCb experiment

2.1 LHC particle accelerator

At CERN, acronym of European Organization for Nuclear Research, located near Geneva in Switzerland, on the French border, is currently operating the largest and most-powerful particle accelerator, the Large Hadron Collider, LHC. It is a synchrotron, built about 100 m underground in a tunnel which has a 27 km long circumference. In it, two proton beams travel in opposite direction with respect to each other in two parallel and adjacent beam pipes, until protons reach an energy of 6.5 TeV each. A strong magnetic field is needed to keep particles flying in circle. Along the ring, there are four collision points, in which the two beams can cross and protons can interact. Protons can be easily produced applying a strong electric field to hydrogen gas, which breaks atoms, stripping away electrons, thus leaving positive ions, i.e. the protons. The continuous flux of protons is then divided into bunches of about 100 billion protons each, spatially separated using a radiofrequency electromagnetic field. The frequency, of about 400 MHz, produces a separation given by

$$\frac{\mathrm{c}}{400\mathrm{MHz}} = \frac{3 \cdot 10^{8}\mathrm{ms}^{-1}}{400 \cdot 10^{6}\mathrm{s}^{-1}} = \frac{3}{4}\mathrm{m}, \tag{2.1}$$

between two adjacent bunches, so the LHC ring could host contemporarily about

$$\frac{27\mathrm{km}}{3/4\mathrm{m}} \approx 36000; \tag{2.2}$$

Anyway, every one bunch, nine are removed and the actual number of bunches is around 2800. These undergo a series of smaller accelerators before entering the LHC ring, where every proton reaches the final energy of 6.5 TeV. The complex of accelerators is schematized in Fig. 2.1.

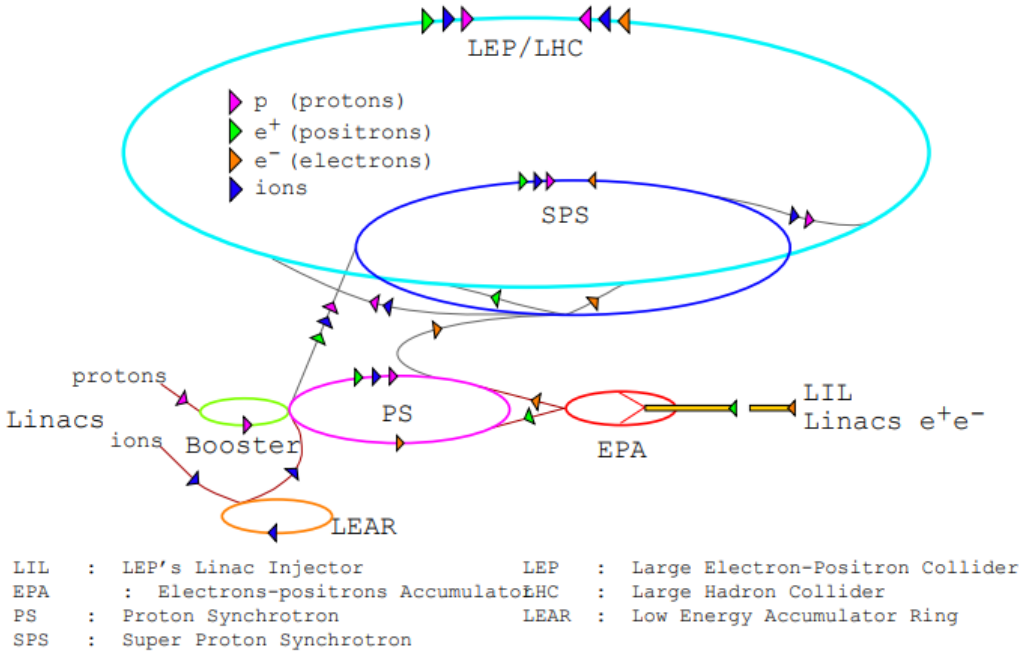

Figure 2.1: Schematic view of the LHC injector complex.

In colliders the centre of mass frame corresponds to the laboratory frame, hence the total momentum in each collision is zero and all the energy, 13 TeV, is available for particles production. Note that these energies are huge; "each proton at the LHC has the kinetic energy of a flying mosquito, and a mosquito has about 10^{20} protons"[1]. The length of a bunch, when accelerated, shorten to 7 cm due to Lorentz contractions. Further assuming a radius of 1 mm, the volume of a bunch can be calculated to be around $V_b = 10^{-4}\text{m}^3$, which is much larger than the volume occupied by 100 billion protons (those contained in a bunch), which can be computed assuming the radius of each proton at rest is of the order of a femtometer, obtaining $V_p = 10^{-37}$ m^3. From the comparison it is clear that each bunch is mostly empty, making collisions extremely rare, that is why a series of quadrupole magnets are used to squeeze bunches up to a few micrometers, thus getting $V_b = 10^{-8}$ m^3, which increases the probability of interactions and so the number of collisions. An important parameter of any accelerator is the luminosity, that is defined as the ratio between the number of detected events in a fixed period of time, dN/dt, and the cross section σ, i.e.

$$L = \frac{1}{\sigma}\frac{dN}{dt}. \tag{2.3}$$

L contains all the parameters related to the collider and the detection system at issue, whereas σ describes the physics of the interaction. The integral over data acquisition

time of L is called integrated luminosity, L_{int}. At CERN there are four main detectors: ATLAS, CMS, LHCb and ALICE; each one is made of many sub-detectors and is built in a different collision point.

2.2 LHCb detector

The goal of LHCb (Large Hadron Collider beauty) experiment[11] is to detect CP violation, small differences between matter and antimatter behaviours, in decaying mesons and baryons that contain beauty or charm quarks. Because of high cross sections, to have enough statistics for LHCb analyses a low average luminosity of about $2 \cdot 10^{32}$ $\mathrm{cm}^{-2}\mathrm{s}^{-1}$ is sufficient. This has also positive side effects: it keep the number of pp collisions per bunch crossing very low, one or two, making it easier to detect them correctly, and furthermore, the lifetime of detecting components is enhanced, since less radiation is produced.

ATLAS and CMS experiments have 4π detectors, i.e. they cover all the solid angle around the interaction point, and so their sub-detectors form a structure similar to the layers of an onion. On the contrary, LHCb experiment exploits the fact that at high energies the majority of interesting hadrons are produced in a forward or backward cone with a small aperture, hence the sub-detectors are placed only in the forward direction and have a planar geometry; for this reason LHCb is referred to as a single-arm spectrometer. It has a forward acceptance from 10 to 250 mrad vertically and 300 mrad horizontally. An overview of the detector can be seen in Fig. 2.2. The coordinate system is chosen with the z-axis aligned horizontally with the beam pipe, while the y-axis is the vertical one.

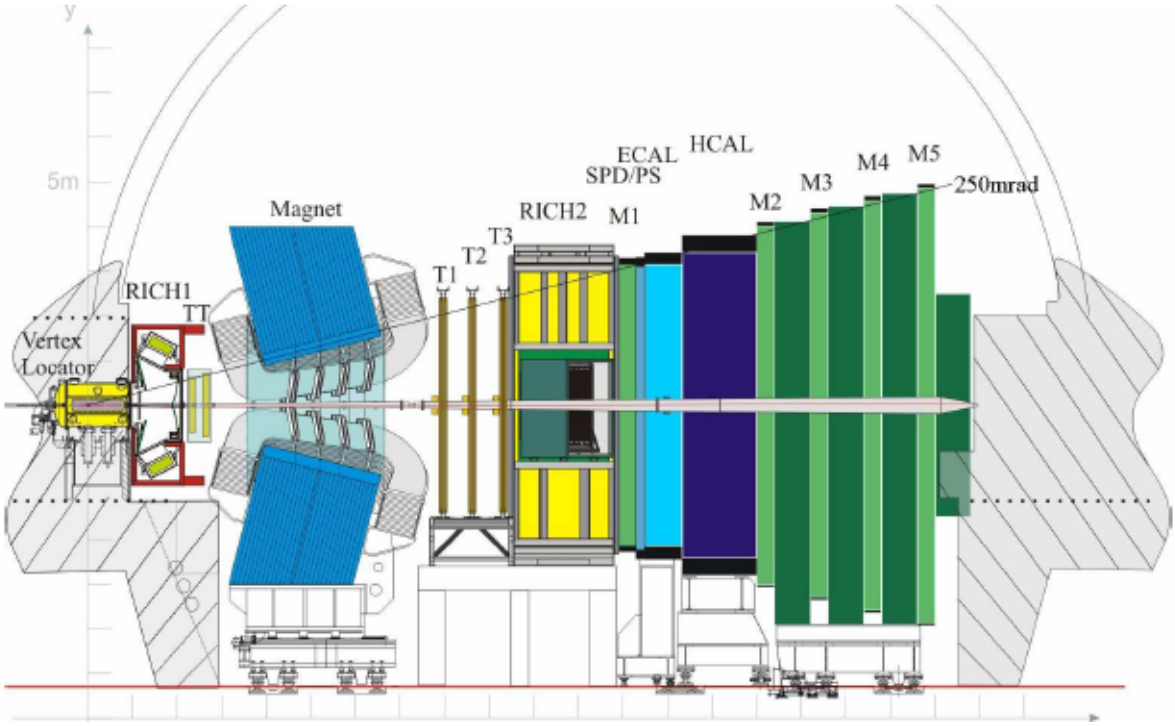

Figure 2.2: View of the LHCb detector.

2.2.1 Tracking system

The tracking system constitutes the part of the detector closest to the interaction point; it is composed by the VErtex LOcator (VELO) and four planar tracking stations, the Tracker Turicensis (TT) in front of the dipole magnet and T1, T2, T3 behind it. VELO is capable of measuring with high precision the coordinates of some points on the trajectory of particles; from these points the tracks can be reconstructed to distinguish secondary vertices from the primary one, so as to locate where b- and c-hadrons are produced and where decay, which allows for a measurement of the decay lifetime.

VELO is made of a series of silicon modules each one divided in two movable halves (left and right of the beam pipe). Each VELO module must return the spatial coordinates: the z-coordinate is simply given by the position of that specific module along the beam pipe, whereas, polar coordinates are used on the x-y plane. To obtain the radius r and the azimuthal angle ϕ, each module half is in turn made of two sensors, the so called R-sensor and ϕ-sensor, placed one in front of the other.

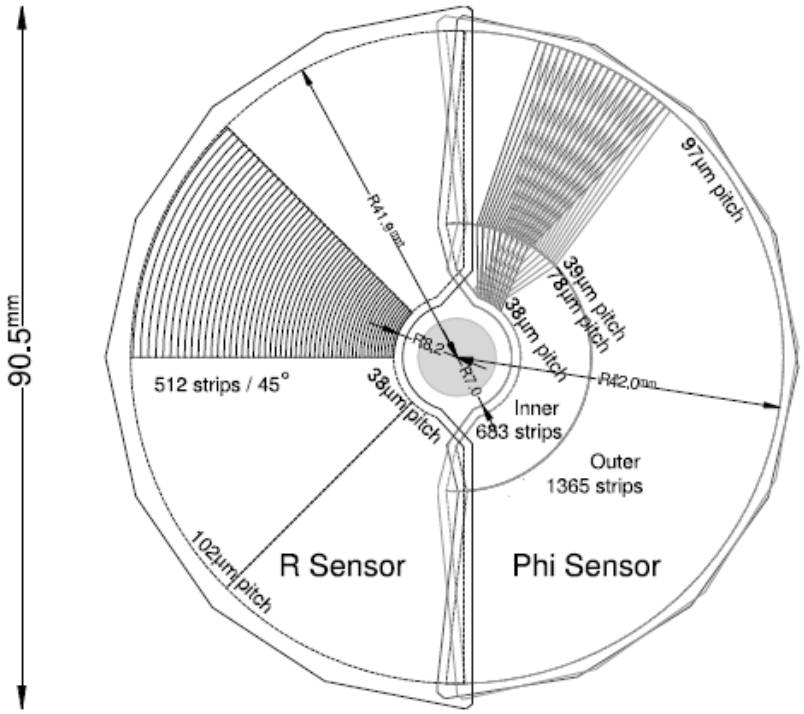

Figure 2.3: Sketch illustrating the geometry of the VELO sensors. For clarity, only a portion of the strips are illustrated.

To build the sensors, silicon microstrip detectors are used; these are arranged in semi-circles in the R-sensor, so that each one is at a fixed distance r from the beam pipe, while the strips are placed radially in the ϕ-sensor. Fig. 2.3 shows how microstrips are positioned in sensors. To minimize the number of strips, the pitch increases from the inside to the outside, i.e. the strips are denser in the inner region.

The second part of the tracking system, in addition to trajectories, can measure also the transverse momentum p_T of charged particles; this is possible thanks to the presence of a vertical magnetic field produced by a dipole magnet, located in between TT and T1, with a bending power about 4 Tm. In order to reduce systematic errors, the orientation of the magnetic field is periodically flipped up and down; charged particles bend on the x-z plane. The equivalence of the Lorentz force and the centripetal acceleration reads

$$\frac{mv^2}{R} = q|\vec{v} \times \vec{B}|; \tag{2.4}$$

recalling that $\vec{B} = B\hat{z}$, one gets

$$p_T = qBR. \tag{2.5}$$

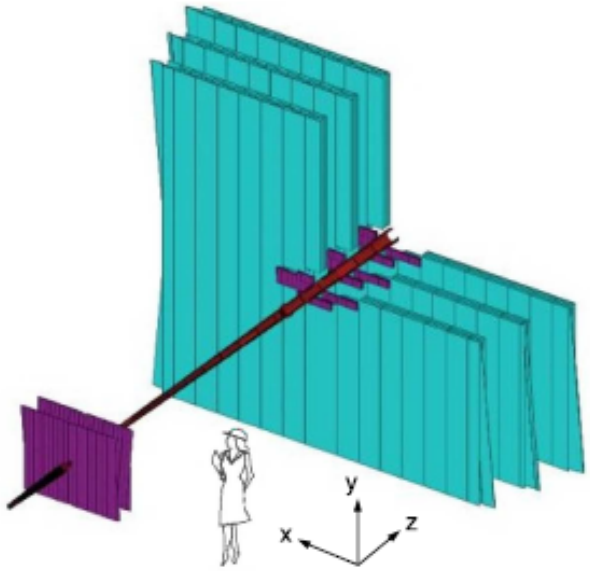

Figure 2.4: Sketch illustrating the geometry of TT, T1-T3 stations and their layers. In purple TT and the inner cross shaped region of T1-T3, which use silicon microstrip detectors. In blue the outer region of T1-T3 which use drift-time detectors.

Fig. 2.4 illustrates the second part of the tracking system. The Tracker Turicensis (TT), and the inner cross shaped region of T1, T2 and T3, close to the beam pipe, use silicon microstrip detectors like VELO. The outer region of the three stations downstream of the magnet use instead a drift-time detectors where straw-tubes are employed to cover a large area. "As gas, a mixture of Ar (70%) and CO_2 (30%) is chosen in order to guarantee a fast drift time"[11]. "Each of the four stations has four detection layers with vertical strips in the first and the last layer and strips rotated by a stereo angle of -5° and +5° in the second and the third layer"[11].

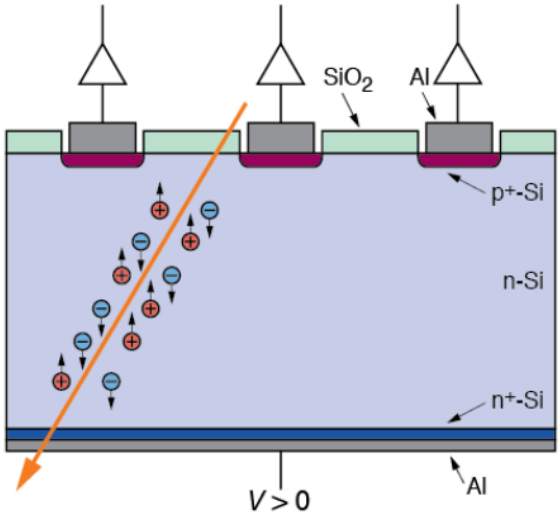

Figure 2.5: Schematic representation of an n-type Si strip detector. A charged particle passes through the detector producing electron-hole pairs.

A schematic representation of a silicon strip detector is given in Fig 2.5. it consists of a n-type silicium substrate and a series of p-type stripes, highly doped, which form several diodes once applied on the substrate. The device is reverse biased (inverse polarisation), so that the central n-type region is fully depleted and there is no leakage current. When a charged particle enters the detector it releases some energy which creates electron-hole pairs; they drift, under the effect of the electric field of the depletion region, towards opposite directions. In Fig. 2.5, it can be seen that holes are pushed towards a certain strip, that collects these charges and produces an electric signal, which gives information about the track of the flying particle. The spatial resolution is extremely high because adjacent strips can be placed with a pitch of the order of 10 μm, hence these detectors are very useful in the region near the interaction point, where they can distinguish between the primary vertex and the near secondary vertexes produces by the decay of charmed and beauty particles. The working principle of a drift chamber instead is much similar to that of a multi-wire proportional chamber, which will be encountered below. Note that, as written above, when passing through the tracking system, each particle spends some of its energy to ionize atoms of the material that it is traversing in order to be detected. However, the energy lost can be calculated using Bethe-Bloch formula and it is found to be just a small fraction of the total energy of the incoming charged particle, so that the calculated value of the transverse momentum is not altered significantly.

2.2.2 Particle identification

Particle identification is essential for the purpose of the experiment; it is realized thanks to the contribution of three parts, Ring-Imaging Cherenkov detectors (RICH), calorimeters and the muon system.

In order to distinguish between pions, kaons and protons, two Ring-Imaging Cherenkov detectors RICH1 and RICH2 are used; two of them are necessary to cover the vast range of possible momenta. RICH1 is located upstream of the magnet to detect charged particles with low momentum, from 1 GeV/c to 60 GeV/c, and to do so it contains aerogel and C_4F_{10} radiators. On the contrary, RICH2 is placed behind the dipole magnet and after T3, and it is used to make the identification of particles with high momenta. To distinguish among them CF_4 is used inside, which is sensitive to momenta in the range 15 GeV/c to 100 GeV/c. Each RICH detector uses a system of mirrors to focus Cherenkov light, produced by the interactions of the incoming particle with the radiator, on Hybrid Photon Detectors (HPDs), placed aside. They can detect Cherenkov photons in the wavelength range 200–600 nm, so as to measure the Cherenkov angle θ_C. An explanation on how this quantity is related to the identification of pions and kaons, can be given looking at the physical phenomenon. Cherenkov radiation is produced in a polarizable material by the passage of a charged particle, which loses part of its energy exciting the molecules of the medium. Then, those molecules relax, emitting photons which classically form spherical wave fronts, originating at each point in space along the particle's trajectory and propagating according to Huygens-Fresnel principle. When the speed v of the charged particle is greater than the speed of light in that medium, given by c/n, where n is the refractive index of the material, interference occurs and the resulting wave front is analogous to "the wave produced by a duck moving on the surface of a pond. The wave front is a triangle with the vertex at the duck, moving forward rigidly with it. The rays of Cherenkov light are directed normally to the V-shaped wave"[3].

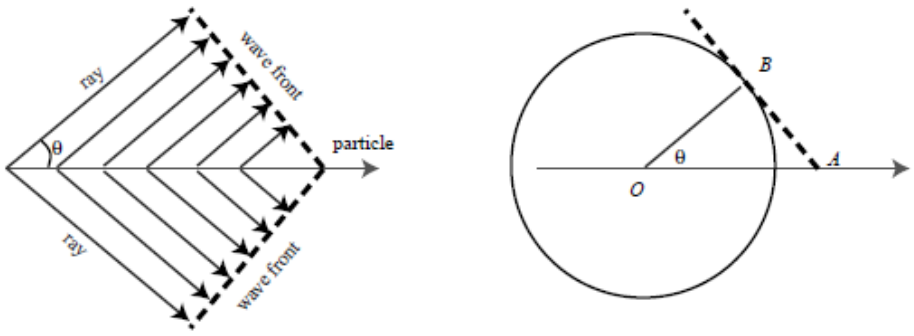

Figure 2.6: Diagrams of Cherenkov wave geometry.

Consider Fig. 2.6, the radius of the spherical wave front originated at $t = 0$ is $OB = ct/n$; in the meanwhile the charged particle has travelled the distance $OA = vt$. Hence,

since OBA is a rectangle triangle, $cos(\theta_C) = OB/OA = 1/\beta n$. This relation can be reversed to obtain β from the measurement of θ_C. Then, if p is measured independently, using the relativistic expression of momentum, $p = m\gamma\beta$, one can get m, which identifies the particle; see Fig. 2.7.

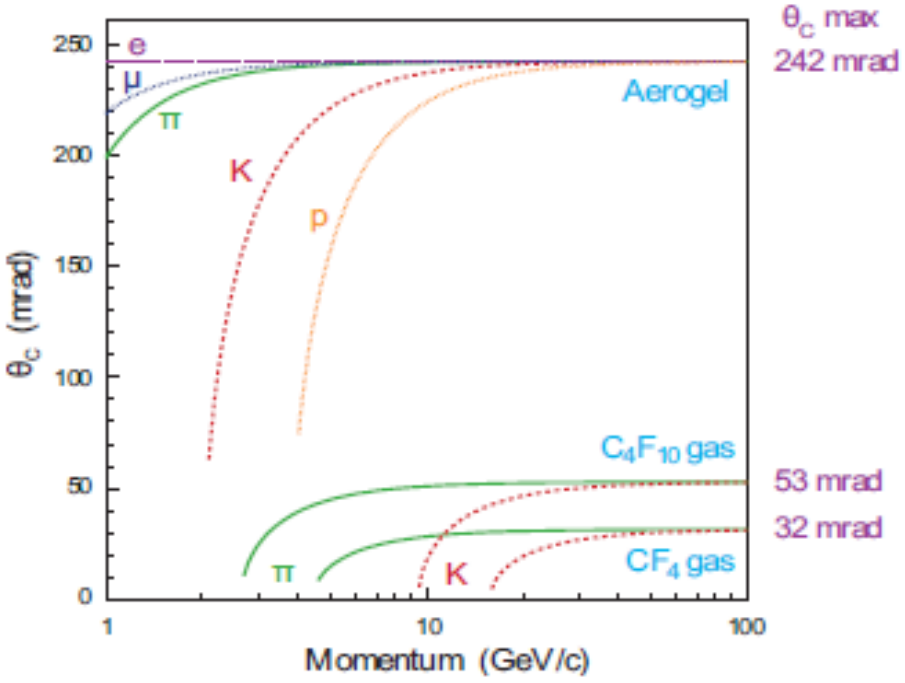

Figure 2.7: Plot of Cherenkov angle versus particle momentum for the RICH radiators. For a fixed momentum of the incoming particle, known from an independent measurement, the value of the angle θ_C distinguishes pions from kaons.

The combination of an Electromagnetic CALorimeter (ECAL), in front, and an Hadron CALorimeter (HCAL), behind, measures the energy of all incoming particles (except for muons and neutrinos); moreover, their longitudinal and transversal segmentation allows to measure the position and to identify the particles. To be specific, the lateral segmentation varies with the distance, the further from the beam pipe, the larger the segmentation, since the hit density varies by two orders of magnitude. All kinds of calorimeter follow the same principle in order to measure energy, that is to stop particles, absorbing all their energy (no leakage outside ideally); for this reason it is called a destructive measurement. An electromagnetic calorimeter is unable to stop hadrons, whereas in an hadron calorimeter photons and electrons would be absorbed without being detected, hence both of them are necessary: the former is sensitive to photons and electrons, while the latter is sensitive to hadrons. Physically what happens inside

an electromagnetic calorimeter is that when an energetic photon ($E_\gamma > 1$ MeV) enters a lead substrate it loses energy mainly by pair production, i.e. creating a couple e^-e^+, while an electron in lead, for $E_e > 10$ MeV, suffers the emission of photons when decelerated (Bremsstrahlung radiation). Hence these two processes, which have respectively the highest cross section in high energy region, leads to the creation of secondary particles; these latter in turn undergo the same processes, giving rise to a third generation of particles and so on; this phenomenon takes the name of electromagnetic shower. Eventually, when the energies of photons and electrons go below the thresholds above-mentioned, they stop producing new particles. Photons continue to lose energy by Compton effect and photoelectric effect, while electron by ionisation and excitation. A completely analogous description could be made for an hadronic calorimeter, where hadrons interact with nuclei instead of with shell electrons of the atoms. Inelastic collisions then produce an hadronic shower. Two parameters can be defined, the radiation length X_0 and the hadron interaction length λ_I, which quantify the distance to travel in a certain material such that the incoming particle is left with a fraction $1/e$ of its initial energy, respectively for an electron in a electromagnetic calorimeter and an hadron in an hadronic calorimeter (the radiation length of a photon is just slightly larger than that of an electron). Many lengths are necessary to have a high energy resolution, i.e. to be almost sure that the particles are truly absorbed. "For this reason, the thickness of ECAL was chosen to be 25 radiation lengths", while "owing to the limited space available, the length of the HCAL has been chosen at $5.6\lambda_I$. The upstream ECAL adds a further $1.2\lambda_I$". This because the hadron interaction length is much larger than the radiation length, which is of the order of centimeters. ECAL and HCAL are sampling calorimeters, i.e. they are composed of an alternation of absorber layers and detection layers; lead and iron are the materials used to produce the showers, respectively in ECAL and HCAL, while both use scintillator detectors in between absorber layers to detect the energy released by the incoming particle. This technology relies on a scintillator material, whose atoms emit photons when struck by ionizing radiation, the light produced is then collected and converted into an electric signal that is measured. With respect to homogeneous calorimeters, sampling calorimeters can be easily segmented and, in addition, both layers are optimized for their purpose; the drawback is that the energy of particles absorbed in the lead/iron layers is not detected. To sum up, sampling calorimeters have worse energy resolution but better position resolution and particle identification.

Muons are found in the final states of many CP-sensitive decays, hence their identification is important. Muons belong to leptons and so they do not interact strongly with the nuclei. In addiction, they are 200 times more massive than electrons, hence they lose much less energy per unit length. This can be understood classically: a heavy body suffers a smaller deceleration when affected by the same force as a light body. Otherwise, looking at the Bethe-Bloch formula one can see that muons start to emit Bremsstrahlung radiation only when $E_\mu > 100$ GeV, which is a much higher threshold when compared to electrons.

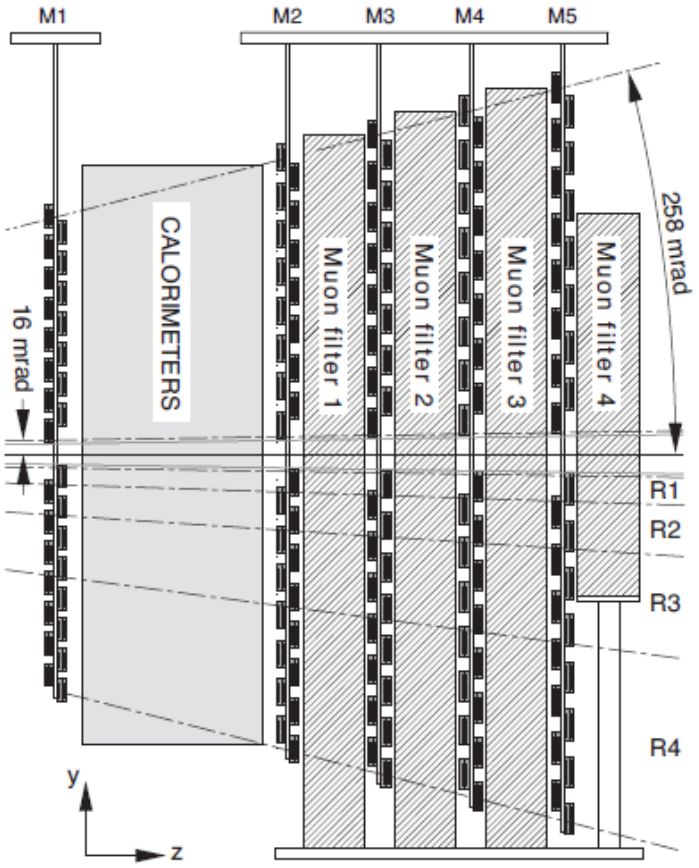

Figure 2.8: Side view of the muon system.

The muon system, illustrated in Fig. 2.8, consists of five stations denoted starting from M1, the most upstream, to M5 and they have a rectangular shape. Station M1 is placed before the calorimeters, while stations M2 to M5 are placed downstream the calorimeters and are separated by 80 cm thick iron absorber layers. Multi-Wire Proportional Chambers (MWPC) are the detectors employed in each station. These detectors provide an electric signal when they are hit by an incoming particle, thus points along the trajectory are obtained. The dimensions of the rectangular partition of each chamber define the x, y resolution. The first three stations have a high spatial resolution along the x coordinate (x-z plane is where the particles bend) so they are used to define the trajectory, whose radius can be used further to calculate the transverse momentum p_T of the candidate muon. Stations M4 and M5 have a lower spatial resolution, so their scope is to identify the penetrating particles, in fact the minimum momentum needed for a muon to cross all the five stations is approximately 6 GeV/c, since the total absorber thickness, which includes also the calorimeters, is approximately 20 interaction lengths.

Each muon station is divided into four regions, named R1 to R4 from the closest to the beam pipe. These four regions have different areas and the chambers used have different dimensions and segmentations too; the correct proportions can be seen in Fig. 2.9, from which it is evident that spatial resolution on the x-y plane gets worse when moving away from the beam pipe.

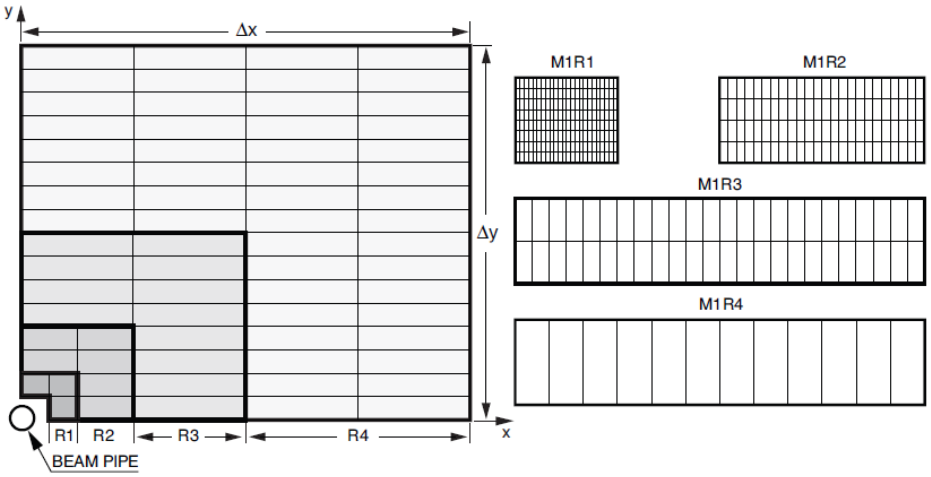

Figure 2.9: Front view of a quadrant of a muon station (left). Each rectangle represents one chamber and each station contains 276 chambers, so each quadrant is made of 69 chambers. On the right, the division into logical pads of four chambers belonging to the four regions of station M1.

A schematic representation of a multi-wire proportional chamber is given in Fig. 2.10, where two parallel cathode planes can be seen (perpendicular to the z-axis), and in between them, a series of wires form the anode, parallel to the x-y plane too. Note that the MWPC is intentionally built perpendicular to the beam direction, i.e. to the incoming particles. The lines of the electric field, which can also be seen in Fig. 2.10, divide the volume of the chamber into longitudinal cells, with a one to one correspondence to the wires. When a charged particle (a muon in the LHCb detector) crosses the cathode plane and enters the chamber, it loses some of its energy to ionise the gas contained there. The resulting free electrons begin to migrate under the effect of the external electric field toward a certain wire, which eventually produces an electric signal. That specific wire gives information about the x coordinate (referring to Fig. 2.10), whereas the z coordinate is given by the anode plane position; in order to get also the y coordinate however, at least another chamber is needed, whose wires must be oriented parallel to the x-axis instead.

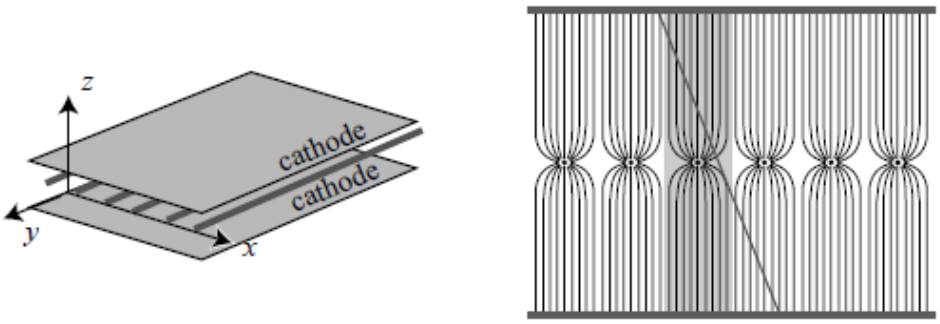

Figure 2.10: Sketch illustrating the geometry of a MWPC.

Chapter 3

Estimation of ΔA_{CP} using semileptonic Λ_c^+ decays

In this thesis work two decay modes of charmed baryon $\Lambda_c^+(ucd)$ are analyzed in order to investigate CP violation in the decay of the particle at issue. Recall that for a charged particle this source of CP violation is the only admissible one. The two channels are

$$\Lambda_c^+ \to p + K^+ + K^- \quad \text{and} \quad \Lambda_c^+ \to p + \pi^+ + \pi^-, \tag{3.1}$$

together with their CP conjugates

$$\overline{\Lambda}_c^- \to \overline{p} + K^+ + K^- \quad \text{and} \quad \overline{\Lambda}_c^- \to \overline{p} + \pi^+ + \pi^-, \tag{3.2}$$

where the two baryons, Λ_c^+ and p, are substituted by the corresponding anti-baryons. For each one of the two channels the CP asymmetry is defined as

$$A_{CP}(f) = \frac{\Gamma\left(\Lambda_c^+ \to f^+\right) - \Gamma\left(\overline{\Lambda}_c^- \to f^-\right)}{\Gamma\left(\Lambda_c^+ \to f^+\right) + \Gamma\left(\overline{\Lambda}_c^- \to f^-\right)}, \tag{3.3}$$

where Γ is the decay width. An asymmetry non compatible with with zero is a sign of CP violation. However, from an experimental point of view, it is not directly measurable. Instead, the signal yields of $\Lambda_c^+ \to p + h^+ + h^-$ and $\overline{\Lambda}_c^- \to \overline{p} + h^+ + h^-$ can be counted (h is a generic label that can be read both as K and as π).

Before doing it, a selection procedure composed of two steps is followed for both data samples. During the pre-selection step, some cuts are applied on the initial dataset to exclude:

- candidates containing misidentified particles,
- clone tracks,

- candidates detected in regions of the experiment with large detection asymmetry,
- contributions from Cabibbo-favoured decays of $\Lambda_c^+ \to p + \pi^+ + \pi^-$ via resonances which do not lead to CP violation.

The second step of the selection consists of a multivariate analysis carried on using Boosted Decision Trees to reduce the combinatorial background.

After the selection procedure, the two signal yields $N^+_{sig}(\Lambda_c^+ \to p + h^+ + h^-)$ and $N^-_{sig}(\overline{\Lambda}_c^- \to \overline{p} + h^+ + h^-)$ can be extracted from the results of a fit to the invariant mass of the final states phh and $\overline{p}hh$ (f^+ and f^-) respectively. The asymmetry that is obtained in this way is called raw asymmetry and it is defined as

$$A_{raw}(f) = \frac{N\left(\Lambda_c^+ \to f^+\right) - N\left(\overline{\Lambda}_c^- \to f^-\right)}{N\left(\Lambda_c^+ \to f^+\right) + N\left(\overline{\Lambda}_c^- \to f^-\right)}. \tag{3.4}$$

Unfortunately $A_{CP}(f)$ and A_{CP}^{raw} do not correspond. The latter is affected also by other sources of asymmetry; at first order these consist of the λ_c^+ production asymmetry $\left(A_{P(\Lambda_c^+)}\right)$ and the p detection asymmetry $\left(A_{D(p)}\right)$. Hence, the raw asymmetry can be expressed as

$$A_{raw}(f) \simeq A_{CP}(f) + A_{P(\Lambda_c^+)}(f) + A_{D(p)}(f). \tag{3.5}$$

Production asymmetry can arise from the greater abundance of quarks with respect to anti-quarks in pp collisions so that more Λ_c^+ are produced than $\overline{\Lambda}_c^-$. Detection asymmetry is caused, for instance, by the fact that anti-protons have larger cross sections for interactions with the detectors, which are made of matter, and thus $\overline{p}$ are detected with higher efficiency when compared to p.

An important assumption is made: production and detection asymmetries depend entirely on the kinematics of particles, respectively of Λ_c^+ and p. For this reason, two decay modes, sharing the two particles, are taken into consideration. In fact, if the kinematics of signal candidates in a decay channel match the kinematics in the other one, then $A_P^{\Lambda_c^+}$ and A_D^P can be considered equal in the two decay modes. Thus, the decay events contained in $\Lambda_c^+ \to p + \pi^+ + \pi^-$ channel are weighted by applying phase-space-dependent weights such that the kinematics matches those in $\Lambda_c^+ \to p + K^+ + K^-$ channel. Consequently, taking the difference between the two raw asymmetries, nuisance asymmetries due to production and detection cancel out. What remains is equal to the difference between the two CP asymmetries in the decays, i.e.

$$\Delta A_{CP}^{wgt} \equiv A_{CP}(pK^+K^-) - A_{CP}^{wgt}(p\pi^+\pi^-) \approx A_{raw}(pK^+K^-) - A_{raw}^{wgt}(p\pi^+\pi^-), \tag{3.6}$$

where A_{CP}^{wgt} and A_{raw}^{wgt} are respectively the CP asymmetry and the raw asymmetry of the weighted sample.

3.1 Data sample selection

The presented analysis uses Run 2 data collected by the LHCb experiment in 2016, obtained from proton-proton collisions at center-of-mass energies of $\sqrt{s} = 13$ TeV, with an integrated luminosity of 0.82 fb^{-1} and magnet down polarity. The total datasets contain about 4.5×10^5 and 1.9×10^6 reconstructed pKK and $p\pi\pi$ signal candidates, respectively.

In pp collisions at LHC, the charmed baryon Λ_c^+ can be the result of prompt production or alternatively, it is a product of the semileptonic decay of the beauty lambda baryon, $\Lambda_b^0 \to \Lambda_c^+ + \mu^- + X$. These secondary vertices are displaced from the primary pp collision due to the relatively long lifetime of Λ_b^0. The dataset used here refers to this latter case. Eventually, Λ_c^+ baryon can decay in the two channels pKK and $p\pi\pi$ directly or through a resonance.

3.1.1 Variables of interest

The quantities used to describe the motion of a particle, i.e. its kinematic in the detector, are three:

- the transverse momentum P_T, i.e. the projection of the momentum vector onto x-y plane. Note that it is a Lorentz invariant quantity for boosts along the z-axis.
- the rapidity y, defined as
$$y \equiv \frac{1}{2} ln(\frac{E + P_z}{E - P_z}), \tag{3.7}$$
where E is the energy of the particle and P_z is the projection of its momentum vector along the z-axis (parallel to the beam pipe). The rapidity is useful because differences of rapidity Δy are Lorentz invariant for boosts along the z-axis. However, it is difficult to measure, so the pseudo-rapidity η is used. It is defined as
$$\eta \equiv -\ln\left(tan(\frac{\theta}{2})\right) = \frac{1}{2} ln(\frac{P + P_z}{P - P_z}), \tag{3.8}$$
where θ is the polar angle, measured with respect to the z-axis. Pseudo-rapidity is actually a proxy at high energies (massless limit) of the rapidity y.
- the azimuthal angle ϕ, the angle on the x-y plane.

3.1.2 Preliminary selection

A first cut is applied on the $Pp\_ProbNNp$ variable, computed by a Neural Network which quantifies the probability that the particle identified as a proton is actually a proton. In the pKK data sample, the misidentification of a pion as a proton implies that D^+ and

D_S^+ are mistakenly selected, because of their decay modes $D^+ \to K^+ + K^- + \pi^+$ and $D_s^+ \to K^+ + K^- + \pi^+$. The lower number of events contained in the pKK data sample makes it the greater component of statistical error on ΔA_{CP}. Hence, the cut on this channel is made to optimize the number of signal events, reducing as much as possible the background due to these mis-id decays. The same cut is applied also to $p\pi\pi$ to not introduce any asymmetry.

In order to optimize the cut, the figure of merit $\frac{S}{\sqrt{S+B}}$ is chosen to be maximized, where S is the number of signal events (Λ_c^+) and B is the sum of events of the two backgrounds (D^+ and D_S^+). The figure of merit is then computed for different value of the cut on the $Pp_Prob NNp$. To obtain the value of S, an invariant mass fit is performed and shown in Fig. 3.1. To compute B, the invariant mass of the three daughters is recomputed (only for those candidates with $Pp_Prob NNp$ lower than the cut value) accounting for the different mass hypothesis on the proton (as a pion) and then fitted to extract the number of D and D_s signal. The resulting invariant mass spectra and fits are shown in Fig. 3.1. Repeating the procedure for different values of the cut, the graph in Fig. 3.2 is obtained, and thus the best cut is found to be $Pp\_ProbNNp > 0.55$.

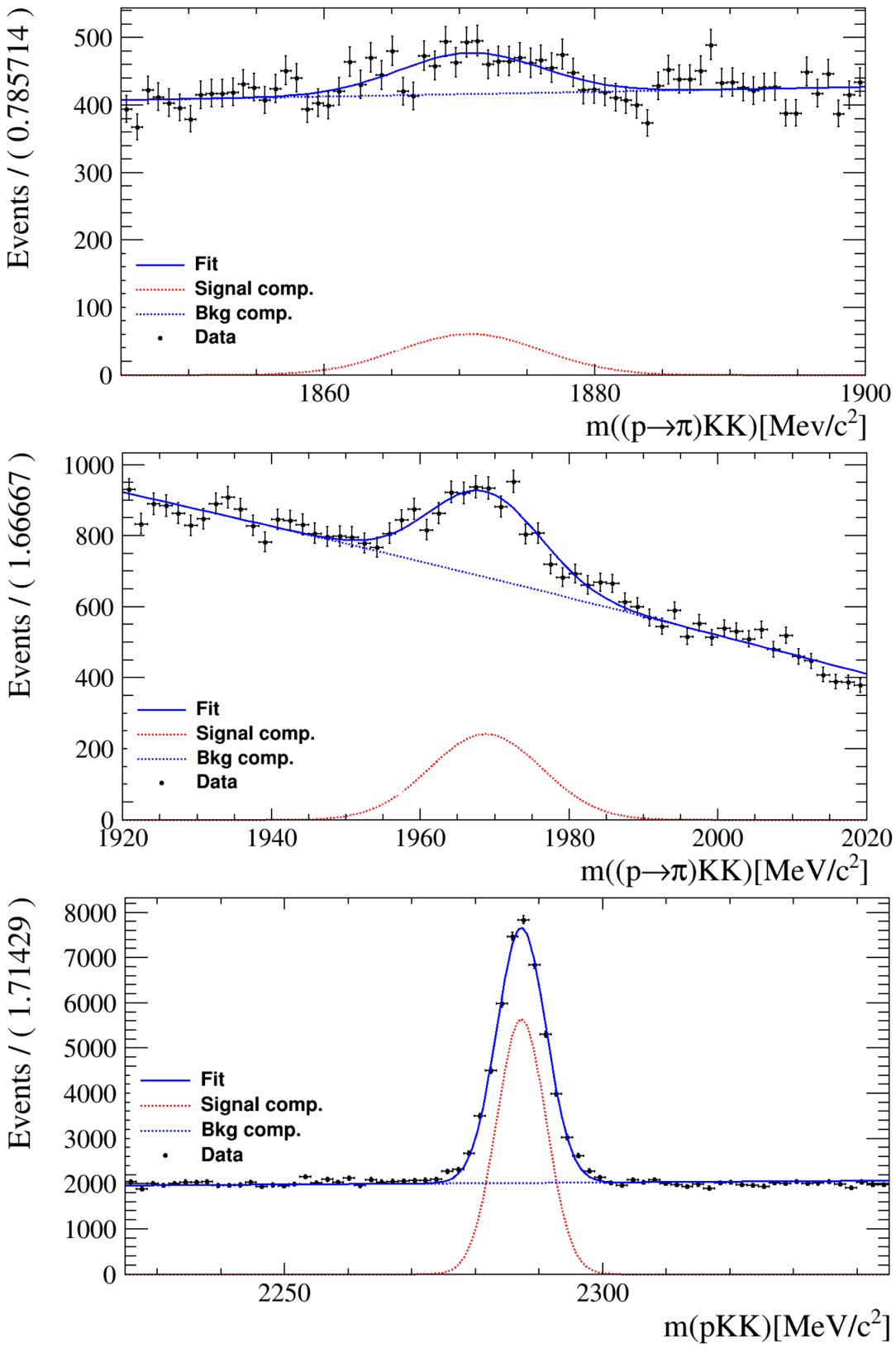

Figure 3.1: Initial distribution of invariant mass of pKK dataset under the hypothesis that events with $Pp\_ProbNNp < 0.55$ are misidentified protons. mis-id protons are given the mass value of a pion. The three ranges of the mass spectrum that are plotted show the peaks of invariant mass of D (top), D_s (middle) and Λ_c (bottom), with fits (blue lines) that determine the number of signal events in each of them.

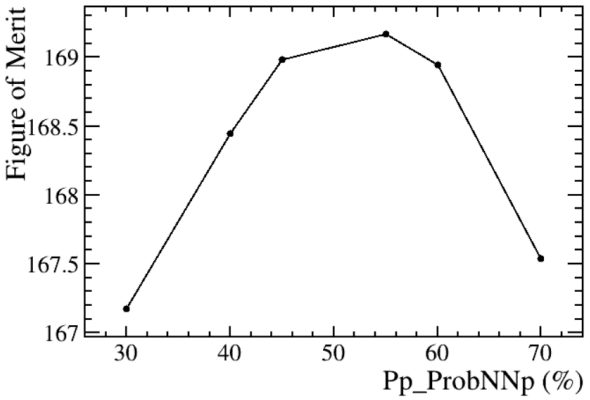

Figure 3.2: Trend of the figure of merit as a function of the cut applied on $Pp\_ProbNNp$.

A second cut is applied simultaneously on $Kp\_ProbNNk$ and $Km\_ProbNNk$ variables on pKK dataset. It reduces the combinatorial background and the background due to pions misidentified as kaons, which cause events belonging to $\Lambda_c^+ \to p + K^- + \pi^+$ decay mode to be selected. The cut is optimized using the same figure of merit as above. For a fixed value of the cut, S is obtained from a Gaussian fit to the invariant mass distribution of pKK as the number of signal events (Λ_c^+), whereas B is given by the number of background events under the peak contained within a 3σ distance from the mean (where 99% of signal events are found). Mean and the sigma values used are the parameters retrieved from the Gaussian fit. Repeating the procedure for different values of the cut, the graph in Fig.3.3 is obtained, and thus the best cut is found to be $Kp\_ProbNNk = Km\_ProbNNk > 0.40$.

Similarly, a cut on $Pip\_ProbNNpi$ and $Pim\_ProbNNpi$ variables is optimized as well. The graph of the figure of merit is shown in Fig.3.3 and the optimal cut is found to be $Pip\_ProbNNpi = Pim\_ProbNNpi > 0.45$.

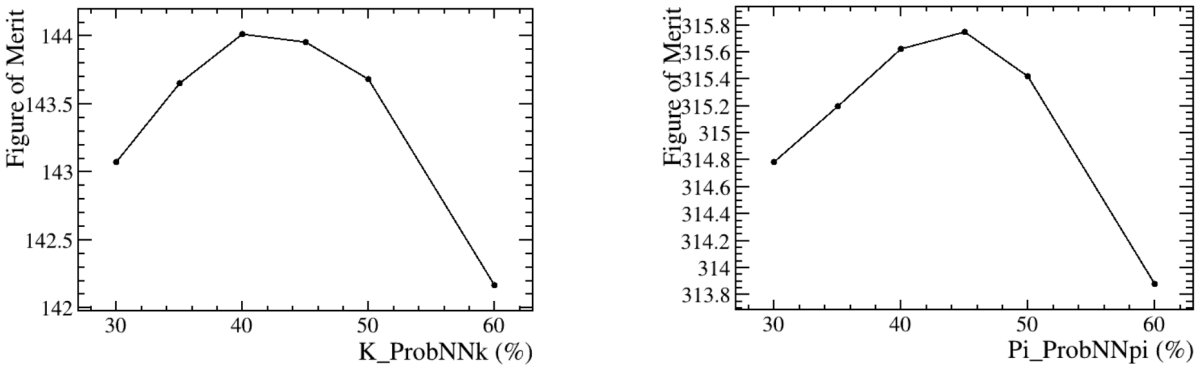

Figure 3.3: Trend of the figure of merit as a function of the cuts applied simultaneously on $Kp\_ProbNNk$, $Km\_ProbNNk$ to pKK dataset (left), and on $Pip\_ProbNNpi$, $Pim\_ProbNNpi$ to $p\pi\pi$ dataset (right).

The cuts applied on the initial distributions on two of these variables are shown in Fig3.4.

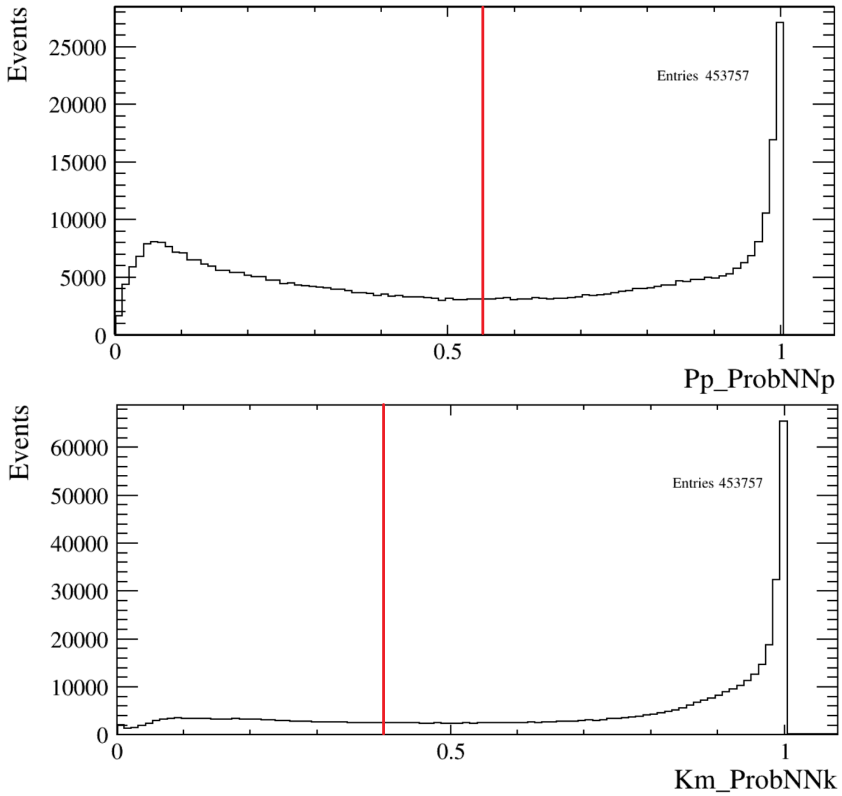

Figure 3.4: Initial distributions of $Pp\_ProbNNp$ (top) $Km\_ProbNNk$ (bottom) of pKK dataset. The vertical red line represents the value of the cut that is applied during preselection step.

The following cuts are also added:

- The angle between two particles produced in the decay must be greater than 0.0008 rad to exclude clone tracks, i.e. one particle that is mistakenly detected as two, flying at a very small angle between each other. It is expressed as

$$\text{acos}(\frac{\vec{P_1} \cdot \vec{P_2}}{P_1 P_2}) > 0.0008, \tag{3.9}$$

  where the couple of labels 1, 2 represents two particle types; the constraint must be applied to all three possible combinations.

- Fiducial cuts to exclude regions of momentum space where the detection asymmetry is high due to the geometry of LHCb detector. The first cut excludes particles detected in the external portion of the detector, at large x-coordinate, where

particles with one charge are bent towards the inside, while the corresponding antiparticles, with opposite charge, are bent towards the outside and thus they are lost. This is expressed as

$$|P_{1,x}| \leq 0.317 \cdot (P_{1,x} - 2000 \text{ MeV/c}), \tag{3.10}$$

where the label 1 represents a particle type; the constraint must be applied to all three particle types in the final state.

The second fiducial cut excludes particles flying in the innermost part of the detector, close to the z-axis, where they can enter the beam pipe and escape undetected.

- Only in the $p\pi\pi$ data sample, two additional cuts must be applied to exclude the Cabibbo-favoured decay modes $\Lambda_c^+ \to p + K_S$ and $\Lambda_c^+ \to \Lambda + \pi^+$. K_S and Λ eventually decay as $K_S \to \pi^+ + \pi^-$ and $\Lambda \to p + \pi^-$, thus result in the same final state of interest, but they do not produce CP violation. To remove from the background their contributions, the following two vetoes are applied on the invariant mass of the couples of particles $\pi\pi$ and $p\pi$,

$$485 < m(\pi^+\pi^-) < 510 \text{ MeV/c}^2 \quad \text{and} \quad 1110 < m(p\pi^-) < 1120 \text{ MeV/c}^2. \tag{3.11}$$

In fact, these are two intervals centered on the mass value of K_s and Λ respectively.

3.1.3 Fitting model

In this section, the model used from now on to fit the invariant mass distribution is presented (the variable is denoted as m). The models $M^\pm$ fit simultaneously the data, divided by charge (Λ_c^+ and $\overline{\Lambda}_c^-$). For both decay channels, the signal components $S^\pm$ are modeled each as the sum of two Gaussian probability density functions (PDFs) of the form

$$Gaussian(m; \mu, \sigma) = \frac{1}{\sqrt{2\pi}\sigma} e^{-\frac{(m-\mu)^2}{2\sigma^2}}. \tag{3.12}$$

The signal components $S^\pm$ have form

$$S^\pm = c^\pm Gaussian_1(m; \mu, \sigma_1^\pm) + (1 - c^\pm) Gaussian_2(m; \mu, \sigma_2^\pm), \tag{3.13}$$

where the mean parameter is the same for all four Gaussians, i.e. they are centered on the same value, whose true value is the invariant mass of Λ_c^+ and $\overline{\Lambda}_c^-$ baryons. However it is not fixed as a constant, to take into account effects caused by the detector.

The background components instead are modeled using a constant PDF for the pKK channel and a first order polynomial PDF for the $p\pi\pi$ channel, respectively

$$B^\pm = Polynomial(m; b_0^\pm) \quad \text{and} \quad B^\pm = Polynomial(m; b_0^\pm, b_1^\pm). \tag{3.14}$$

Rather than directly fitting charge-dependent signal and background yields, denoted respectively as $N_{sig}^{\pm}$ and $N_{bkg}^{\pm}$, they are expressed using the total number of signal and background events, N_{sig} and N_{bkg}, and the signal and background asymmetries, A_{raw} and $A_{raw,bkg}$. So, the combination of signal and background results in

$$M^{\pm}(m;\mu,\sigma_1^{\pm},\sigma_2^{\pm},b_i^{\pm}) = N_{sig}^{\pm}S^{\pm}(m;\mu,\sigma_1^{\pm},\sigma_2^{\pm}) + N_{bkg}^{\pm}B^{\pm}(m;b_i^{\pm}), \tag{3.15}$$

where $i = 0$ for pKK sample or $i = 0, 1$ for $p\pi\pi$ sample, and

$$N_{sig}^{\pm} = \frac{1}{2}N_{sig}(1 \pm A_{raw}) \quad \text{while} \quad N_{bkg}^{\pm} = \frac{1}{2}N_{bkg}(1 \pm A_{raw,bkg}). \tag{3.16}$$

To ensure that only the events containing positively charged baryons (Λ_c^+, p) are assigned to M^+ and only those containing negatively charged anti-baryons ($\overline{\Lambda}_c^-$, $\overline{p}$) are assigned to M^-, Dirac delta functions are included into $M^{\pm}$. So, $M^{\pm}$ become

$$M^{\pm}(m, ID;\mu,\sigma_1^{\pm},\sigma_2^{\pm},b_i^{\pm}) = \delta^{\pm}(ID)[N_{sig}^{\pm}S^{\pm}(m;\mu,\sigma_1^{\pm},\sigma_2^{\pm}) + N_{sig}^{\pm}B^{\pm}(m;b_i^{\pm})], \tag{3.17}$$

where the Dirac delta functions $\delta^{\pm}$ act on the two-valued discrete variable Lc_ID (or equivalently Pp_ID, because Λ_c and p must have the same charge), and select only the events tagged with the correct electric charge. In this way, the two pieces $M^{\pm}$ can be put together, building the total PDF

$$M(m;\vec{\alpha}) = M^+(m;\mu,\sigma_1^+,\sigma_2^+,b_i^+) + M^-(m;\mu,\sigma_1^-,\sigma_2^-,b_i^-), \tag{3.18}$$

where the vector $\vec{\alpha}$ collects all the parameters.

3.1.4 Background reduction

The sPlot procedure uses the fit to the invariant mass distributions of pKK and $p\pi\pi$ datasets that result from the preliminary selection to compute two distinct weights (referred to as *s-weights*) for each event. This is done using `RooStats::SPlot` class in ROOT. If one of the two kinds of *s-weights* is applied to all the events of the sample, the distribution appears either as pure signal or pure background. The two weights show separately the two different components (signal and background) of the distribution. Note that events are not sorted into signal or background, i.e. no cuts are applied; rather, all events are present in both cases. Fig.3.5 shows the scatter plot for $s-weights$ for signal events in function of the invariant mass of pKK dataset.

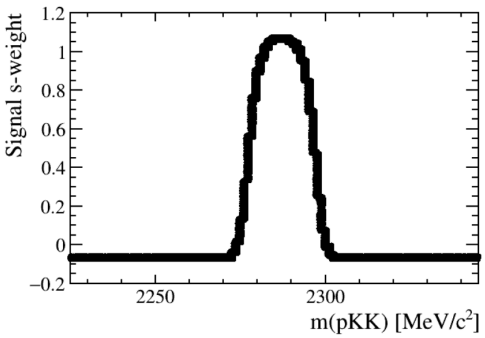

Figure 3.5: Scatter plot for $s-weights$ for signal events in function of the invariant mass of pKK dataset.

In order to reduce the background, a multivariate analysis is conducted using a machine learning technique, the Boosted Decision Trees (BDT). The corresponding method is booked using TMVA class (with ROOT), designed specifically for training and classification with multivariate methods. Signal and background samples are needed; they must be separate. Instead of using Monte Carlo simulations, the *s-weights* obtained in the previous step are applied to pKK and $p\pi\pi$ datasets to get pure signal and pure background distributions for both. In turn, each of them (signal and background samples) is split into two halves, one is used for training and the other for testing the consistency of the method, against statistic fluctuations. Hence, BDT is trained on real data.

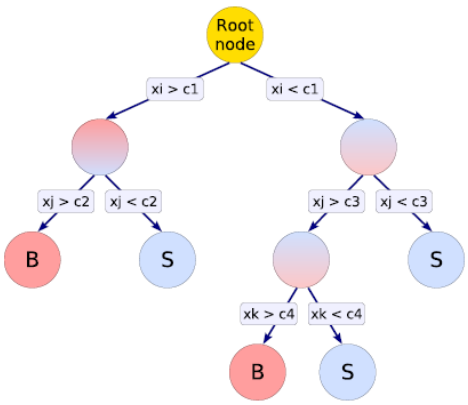

Figure 3.6: Schematic view of a decision tree. Starting from the root node, a sequence of binary splits using the discriminating variables xi is applied to the data. Each split uses the variable that at this node gives the best separation between signal and background when being cut on. The same variable may thus be used at several nodes, while others might not be used at all. The leaf nodes at the bottom end of the tree are labeled S for signal and B for background depending on the majority of events that end up in the respective nodes.

Each decision tree is a binary structured classifier, whose functioning is schematized in Fig.3.6. It divides the phase space originated by the variables given as input to the BDT into disjoint regions. Each region is classified as background region or signal region. The choice depends on whether the majority of events contained in there belongs to the background training sample or the signal training sample, respectively. The term *boosted* refers to the fact that not only one tree is used, but rather a forest (N=400). Each tree bases its decisions on the training data sample, but the events are re-weighted differently. In the end, each event is classified on a majority vote of the classifications done by each tree in the forest. A new variable is defined, the *BDT response*, and a value is assigned to each event of the two samples (signal and background). *BDT response* variable lies between -1 and $+1$. An ideal result would be to have all signal events with *BDT response*$= +1$ and all background events with *BDT response*$= -1$.

The training is followed by the testing phase. The same procedure is applied to the second half of signal and background samples. These are independent data samples; therefore, a good agreement with the distributions of the *BDT response* obtained during the testing phase proves that it is not heavily affected by statistical fluctuations. It can further evaluate the performances of the classification and monitor the overtraining.

The distributions of the variables of the pKK channel used to train the BDT are represented in Fig.3.7, where they are divided into signal and background samples. The correlation matrix between these variables is reported in Fig.3.8. The distributions of *BDT response* variable in the two samples (signal and background) of pKK channel after the training is shown in Fig.3.9.

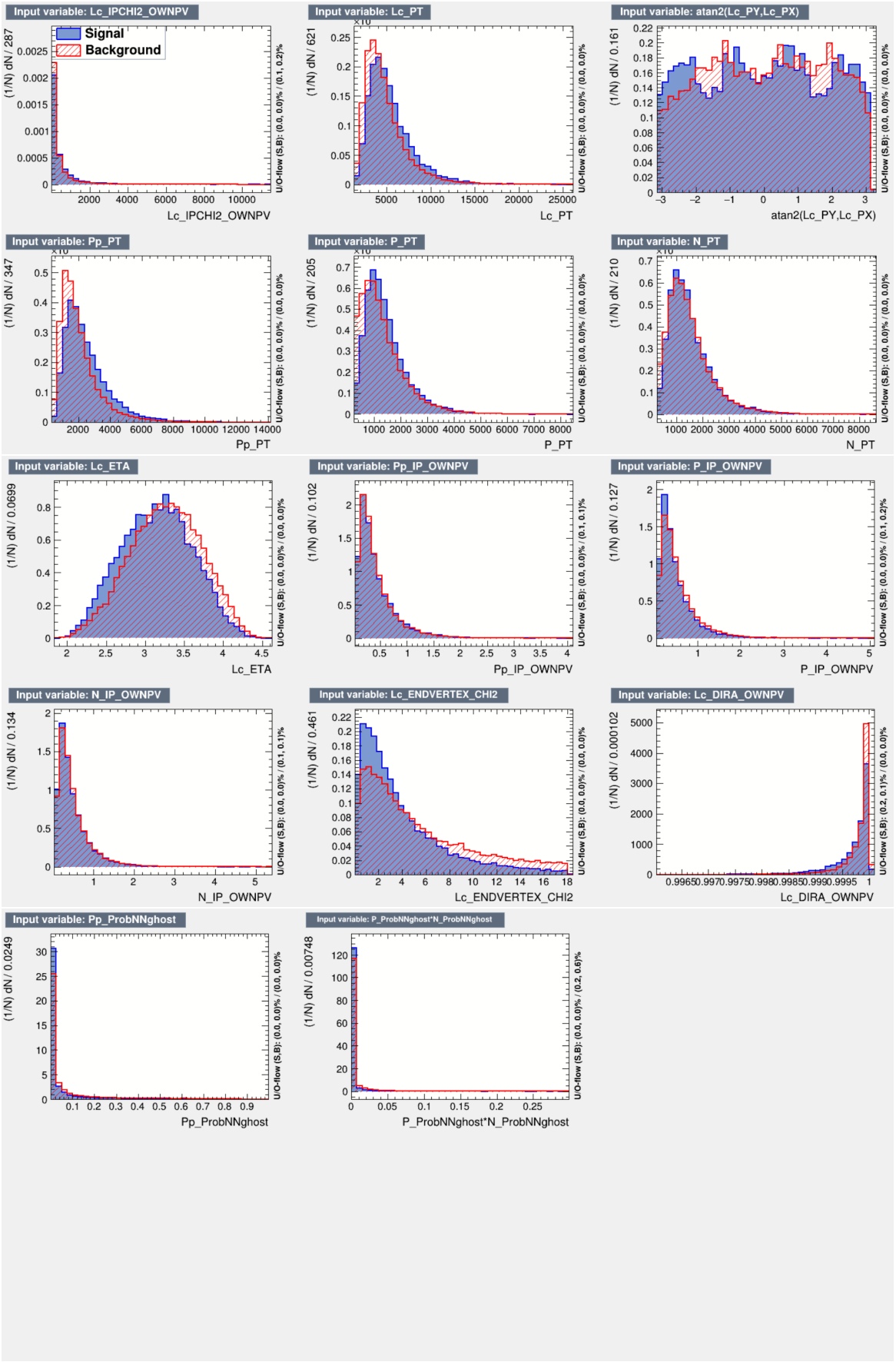

Figure 3.7: Distributions of the variables of the pKK dataset used to train the BDT. They are divided into signal and background samples using the corresponding $s-weights$.

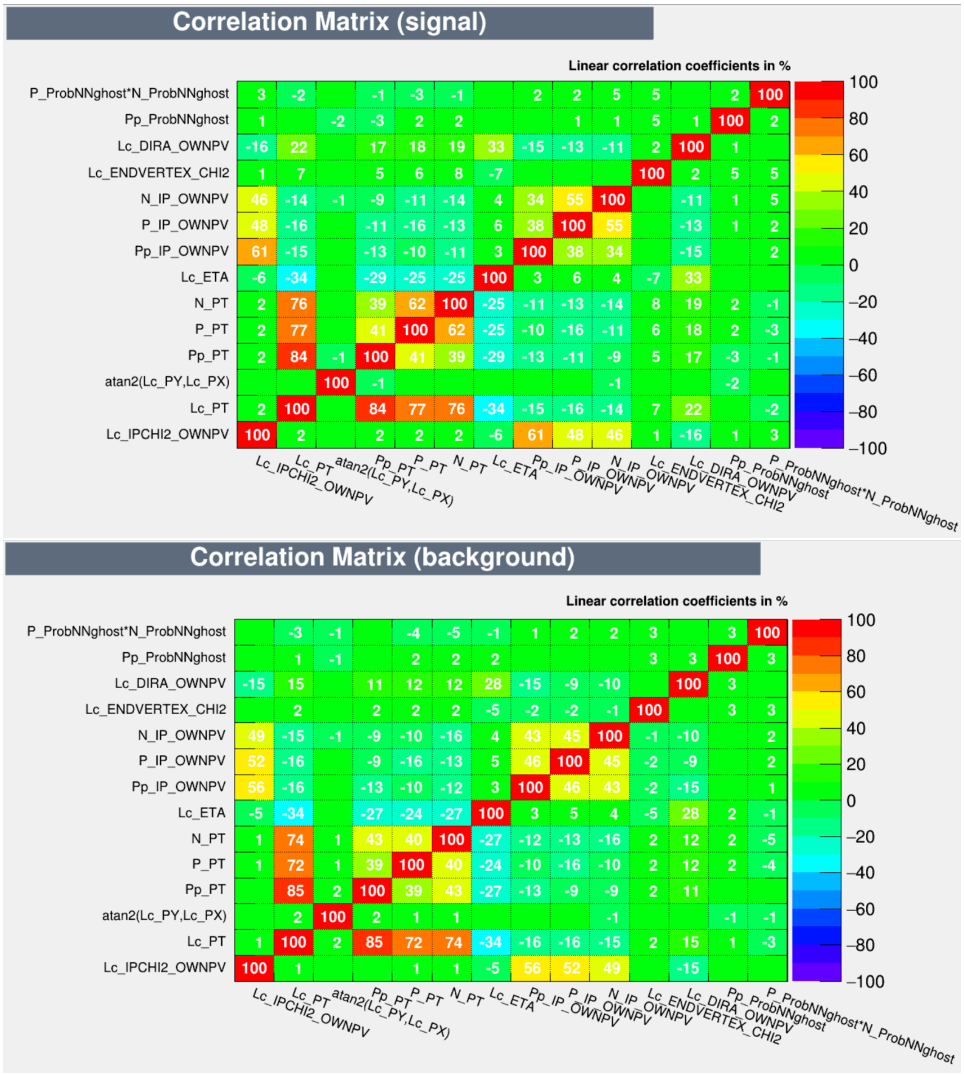

Figure 3.8: Correlation matrices between the input variables for signal data sample (top) and background data sample (bottom), taken from pKK dataset.

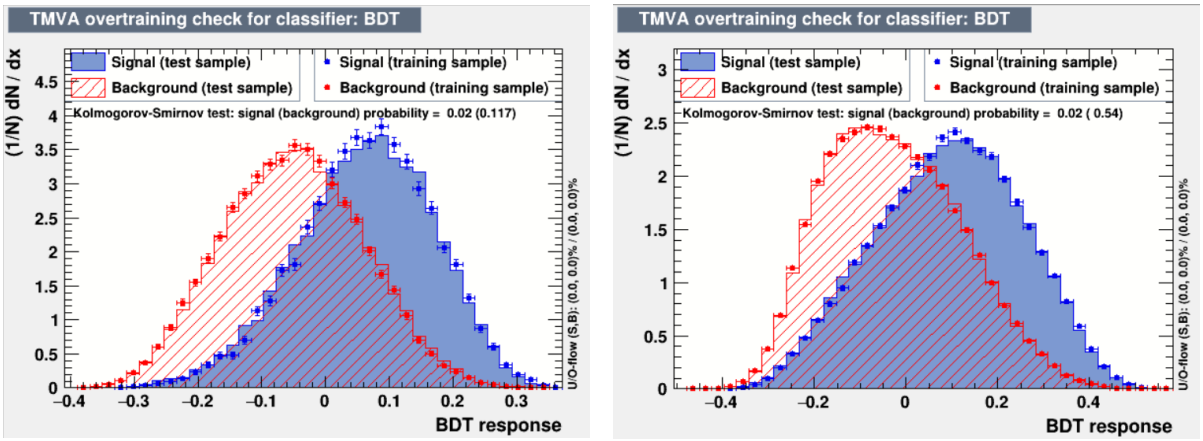

Figure 3.9: Distribution of the *BDT response* in pKK dataset (left) and $p\pi\pi$ dataset (right).

After training and testing are completed, and executed independently between pKK and $p\pi\pi$, the BDT can be used to classify pKK and $p\pi\pi$ datasets. A *BDT response* value is assigned to each event. Finally, applying a cut on this variable background is reduced. To optimize the cut, its efficiency is calculated on the testing samples (signal and background), separately, as

$$\epsilon_{sig(bkg)} = \frac{\#signal\ (background)\ events\ after\ cut}{\#signal\ (background)\ events\ before\ cut}. \tag{3.19}$$

Fitting pKK and $p\pi\pi$ datasets with model 3.18 the parameters are obtained. Signal and background yields N_{sig}, N_{bkg} are multiplied by the correspondent efficiency ϵ_{sig}, ϵ_{bkg} to simulate the PDF of invariant mass after the cut. The updated PDF is used to generate a new set of data, which is fitted again with model 3.18. The value of the error associated to the signal asymmetry A_{raw} is plotted on the graph reported in Fig.3.10 for the pKK sample. The optimized cuts are those that minimize the statistical uncertainty of the raw asymmetry, which result to be $BDT\ response > -0.125$ for pKK channel and $BDT\ response > -0.2$ for $p\pi\pi$ channel.

A comparison between the initial distributions of invariant mass of pKK, $p\pi\pi$ datasets and what is left after the selection process is shown in Fig.3.11, where the two of them are plotted on the same frame. Ideally, the background component should be strongly reduced whereas the signal component should appear approximately identical.

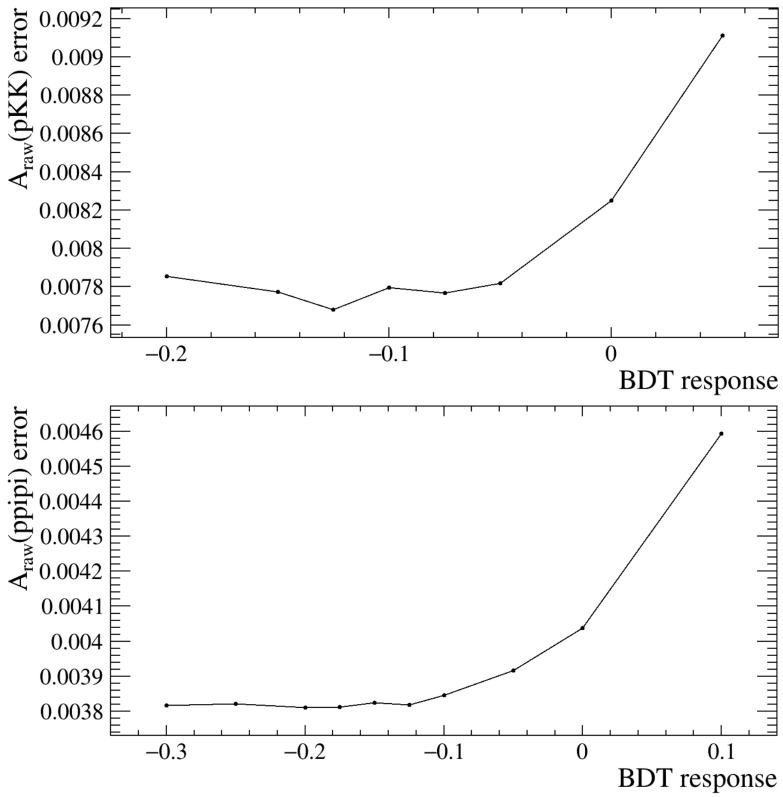

Figure 3.10: Trend of the error on raw asymmetry as a function of the cut applied to the *BDT response* on pKK dataset (top) and $p\pi\pi$ dataset (bottom). The raw asymmetry and the corresponding uncertainty are obtained from the fit to a data sample generated according to the same distribution as the true data, but signal and background yields are modified to reflect the efficiencies of the cut on each of the two components.

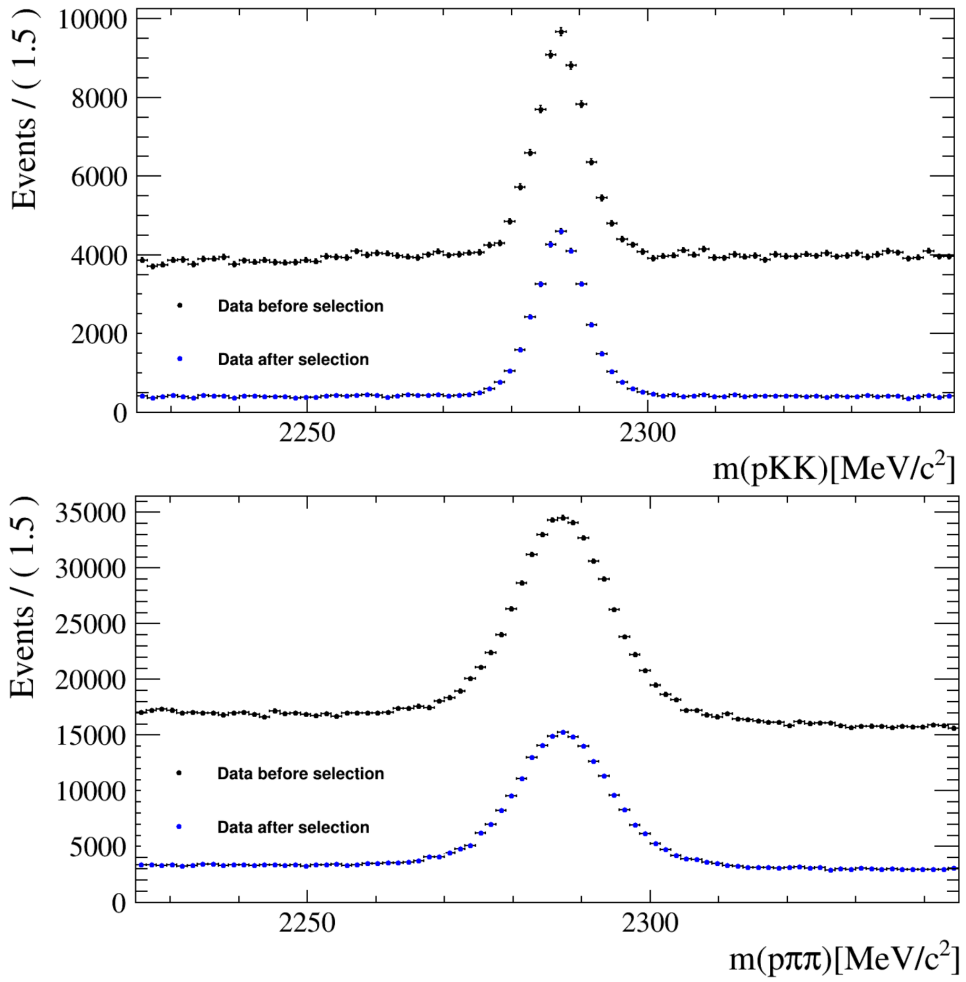

Figure 3.11: Invariant mass distribution before and after the selection step in pKK dataset (top) and $p\pi\pi$ dataset (bottom).

3.2 Weighting procedure

The following step of the analysis is the weighting procedure, which assigns a kinematic weight to each event of $\Lambda_c^+ \to p + \pi^+\pi^-$ decay channel (since the weighting procedure increases our statistical error), so that the distributions of kinematic variables of the signal component of this channel match those of signal candidates of $\Lambda_c^+ \to p + K^+ + K^-$ decay channel. Weights are applied to $p\pi\pi$ sample because of its higher statistics, so that the dominant contribution to the uncertainty on ΔA_{CP}^{wgt}, that is the statistical uncertainty associated to the raw asymmetry in pKK sample, is left untouched.

Recall that the kinematic of a particle is describe by three variables: the transverse momentum P_T, the pseudo-rapidity η and the azimuthal angle ϕ. The distribution of

each kinematic variable of Λ_c^+ and p is shown in Fig.3.12, where the two histograms are overlapped to simplify the comparison. The events are weighted using the *s-weights*, so that the distributions refer to the signal component only. From Fig.3.12 it is evident that the superposition is not precise, so that the weighting procedure is needed.

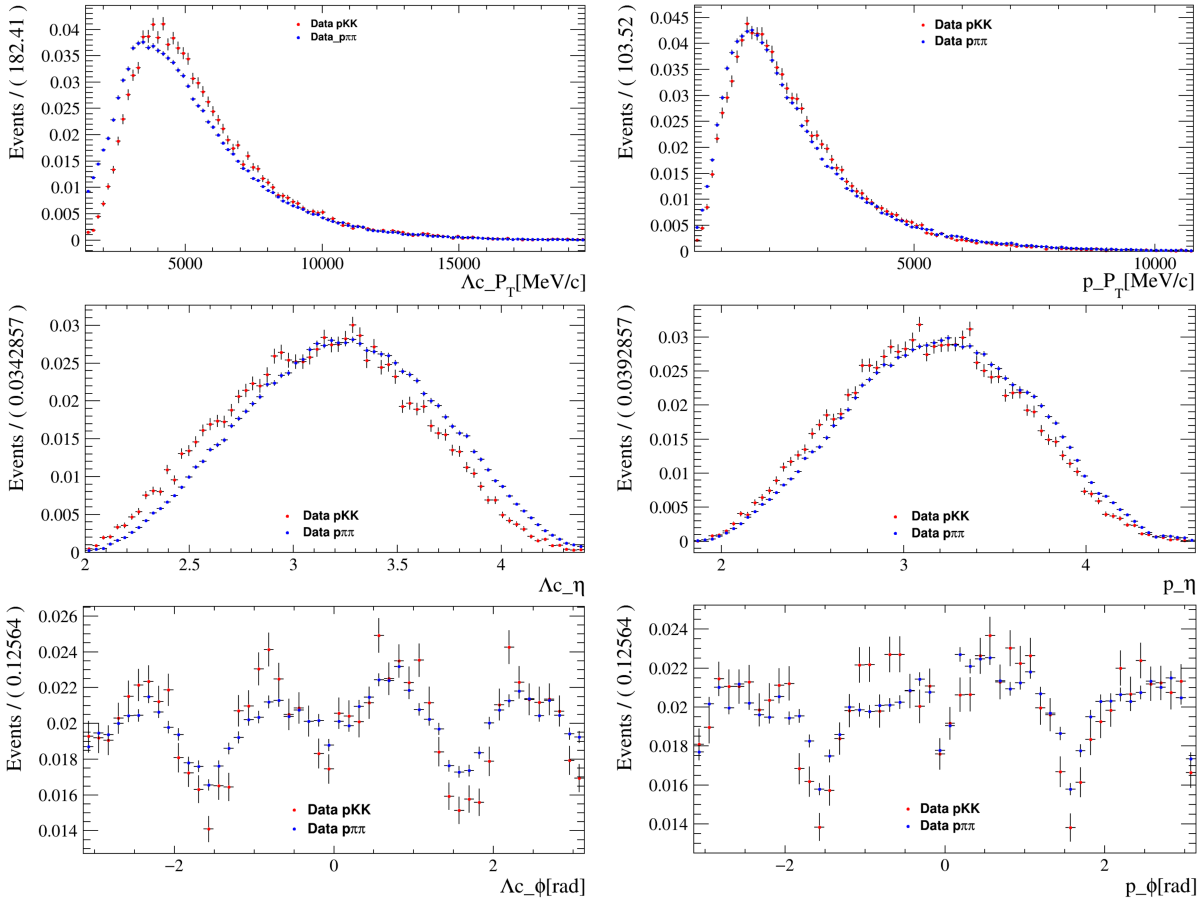

Figure 3.12: Initial distributions of the kinematic variables.

The procedure runs iteratively and the variables are considered one at a time in the following order: *Lc_PT*, *Lc_ETA*, *Lc_PHI*, *Pp_PT*, *Pp_ETA*, *Pp_PHI*. At each step the division between the two weighted histograms that refer to the same kinematic variable is done; notice that in order to obtain valid results from a division, the two histograms must have the same range, same number of bins and no empty bins. The resulting value of each bin represents a weight, that is associated to all the events contained in that specific bin. At the *j-th* iteration, the weight associated to the events in the *i-th* bin is

$$\omega_i^{(j)} = \frac{N(p\pi\pi)N_i^{bin}(pKK)}{N(pKK)N_i^{bin}(p\pi\pi)}, \tag{3.20}$$

where $N(p\pi\pi)$, $N(pKK)$ are the total number of events contained in the samples, whereas $N_i^{bin}(pKK)$ and $N_i^{bin}(p\pi\pi)$ are the events contained in the *i-th* bin. The factor $\frac{N(p\pi\pi)}{N(pKK)}$ comes from the normalization to 1 of the two histograms. Before moving to the next step, each event is re-weighted; this preliminary weight is calculated multiplying the *s-weight* by all the j weights associated to that event (one per each step) up to that point.

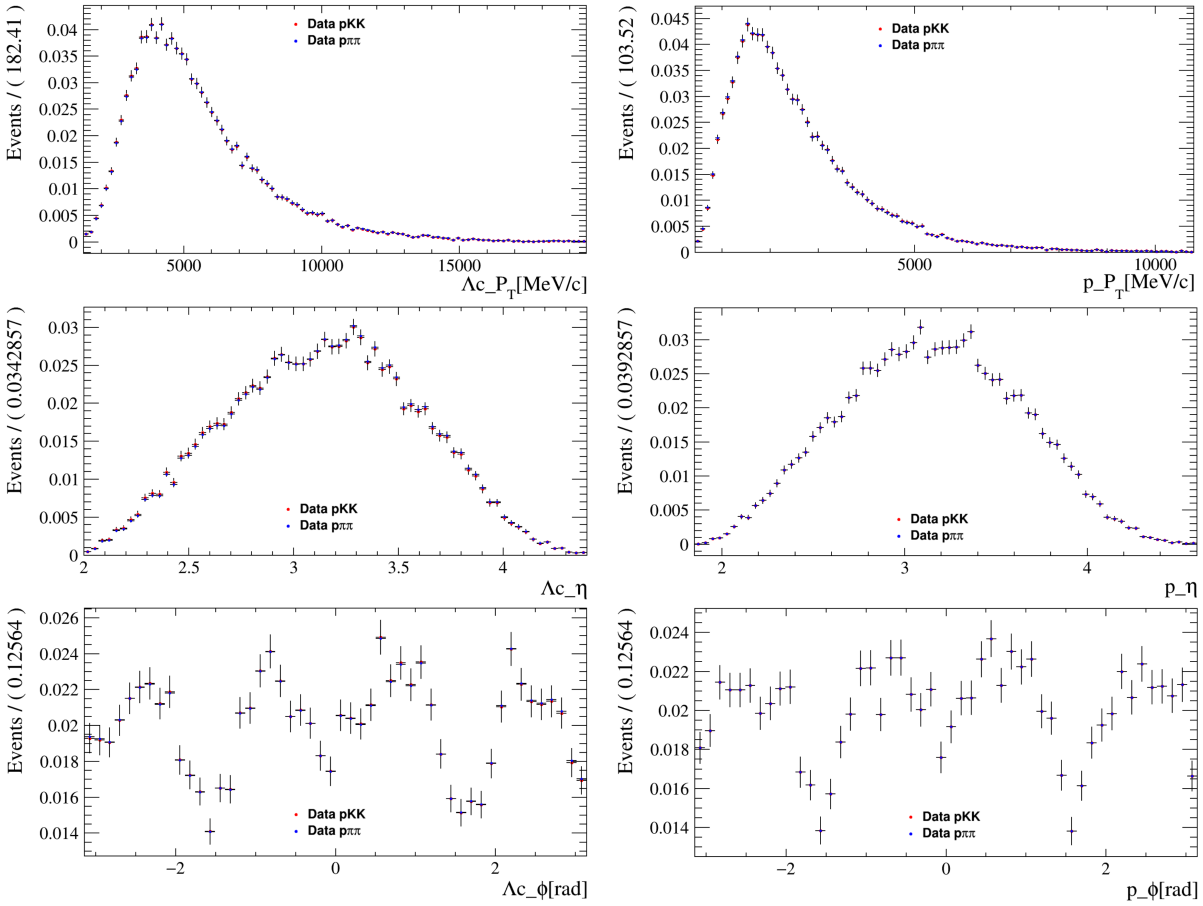

Figure 3.13: Final distributions of the kinematic variables. Preliminary weights are applied to $p\pi\pi$ dataset.

The procedure is iterated for 10 loops over all six variables; the resulting histograms are shown in Fig.3.13, to be compared with the initial one. The kinematic weight ω_n that is associated to the *n-th* event corresponds to the product of all the weights obtained at each step

$$\omega_n = \prod_{j=1}^{60} \omega_n^{(j)}, \tag{3.21}$$

where $\omega_n^{(j)}$ is the weight associated to the *n-th* event during step number j. Note that the *s-weights* are not included in the computation of the kinematic weights. Normalized kinematic weights ω_n^{norm} are then computed using

$$\omega_n^{norm} = \frac{\omega_n}{\omega^{norm}}, \tag{3.22}$$

where ω^{norm} is defined as

$$\omega^{norm} \equiv \frac{\sum_n \omega_n}{N_{tot}}. \tag{3.23}$$

Normalized kinematic weights are plotted in Fig.. The distribution is centered on 1. In fact, if the kinematics in the two channels were equal, it would be precisely a Dirac delta. On the contrary, the greater is the distribution's width, the more the two kinematics differ from each other.

3.3 Results

The fitting model 3.18 is applied to both pKK and $p\pi\pi$ data samples; this latter is weighted using normalized kinematic weights ω_n^{norm} previously calculated. Fig.3.14 and Fig.3.15 show the distributions of invariant mass divided by electric charge and the model fitted to each subset of data.

The resulting raw asymmetries are obtained:

$$A_{raw}(pK^+K^-) = (2.4 \pm 0.8)\%, \tag{3.24}$$

$$A_{raw}^{wgt}(p\pi^+\pi^-) = (2.6 \pm 0.5)\%. \tag{3.25}$$

Thus, the difference of CP violation in the two decay channels $\Lambda_c^+ \to p + K^+ + K^-$ and $\Lambda_c^+ \to p + \pi^+ + \pi^-$ can be calculated according to Eq. 3.6. The result is

$$\Delta A_{CP}^{wgt} = (-0.2 \pm 0.9)\%, \tag{3.26}$$

which is compatible with zero. The uncertainty is evaluated using the sum of squared errors. To do so, the uncertainties associated to the two raw asymmetries must be casual and independent. The Gaussian shape of signal distributions suggests that fluctuations are casual. Beside, the probability that both kaons are simultaneously misidentified as pions (or vice versa) is extremely low, so, we can assume no events are contained in both datasets, which can be considered independent.

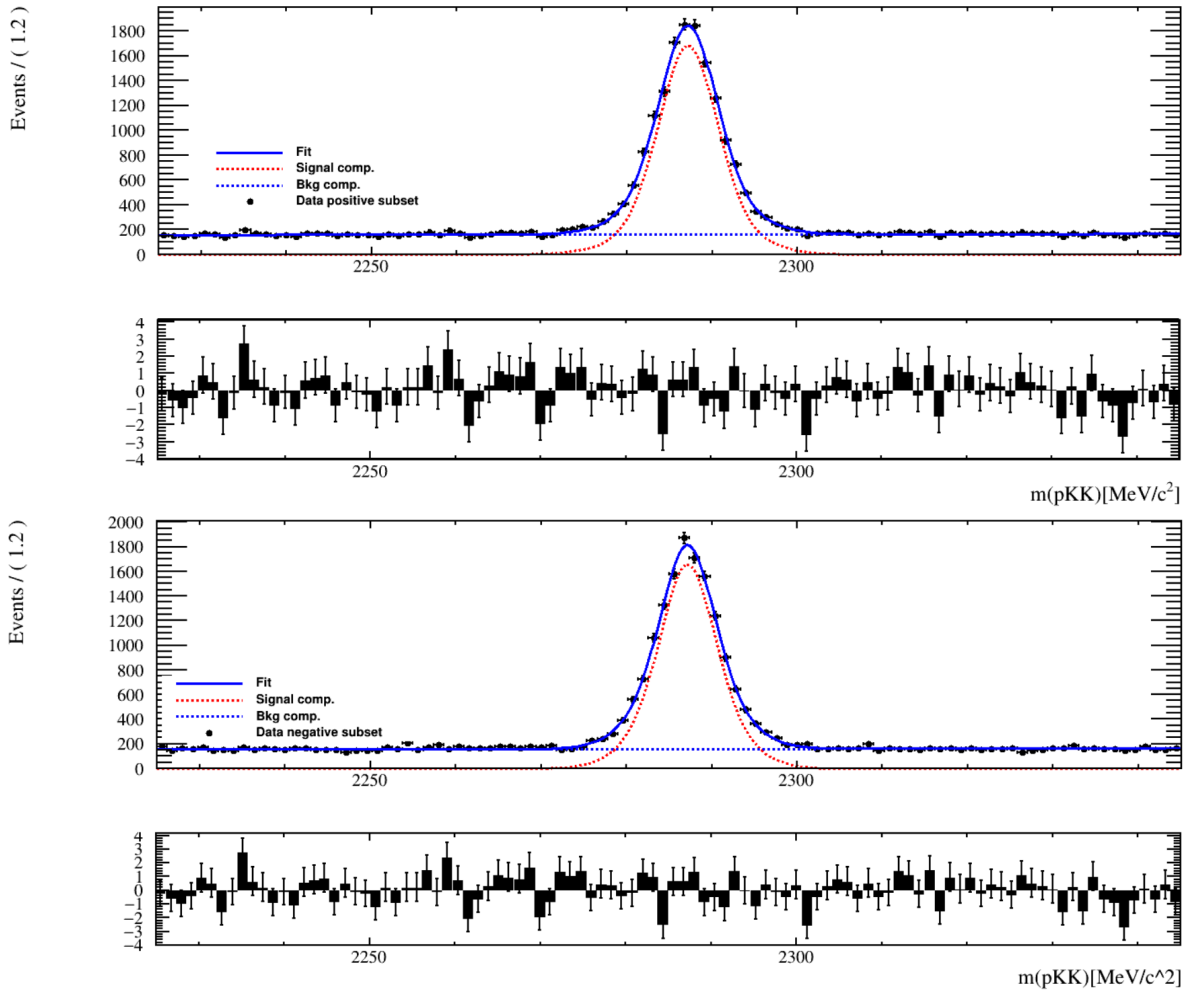

Figure 3.14: Invariant mass distribution of the two subsets of pKK dataset, containing respectively positively charged protons (top) and negatively charged anti-protons (bottom). The fits used for the determination of raw asymmetry are superimposed to data.

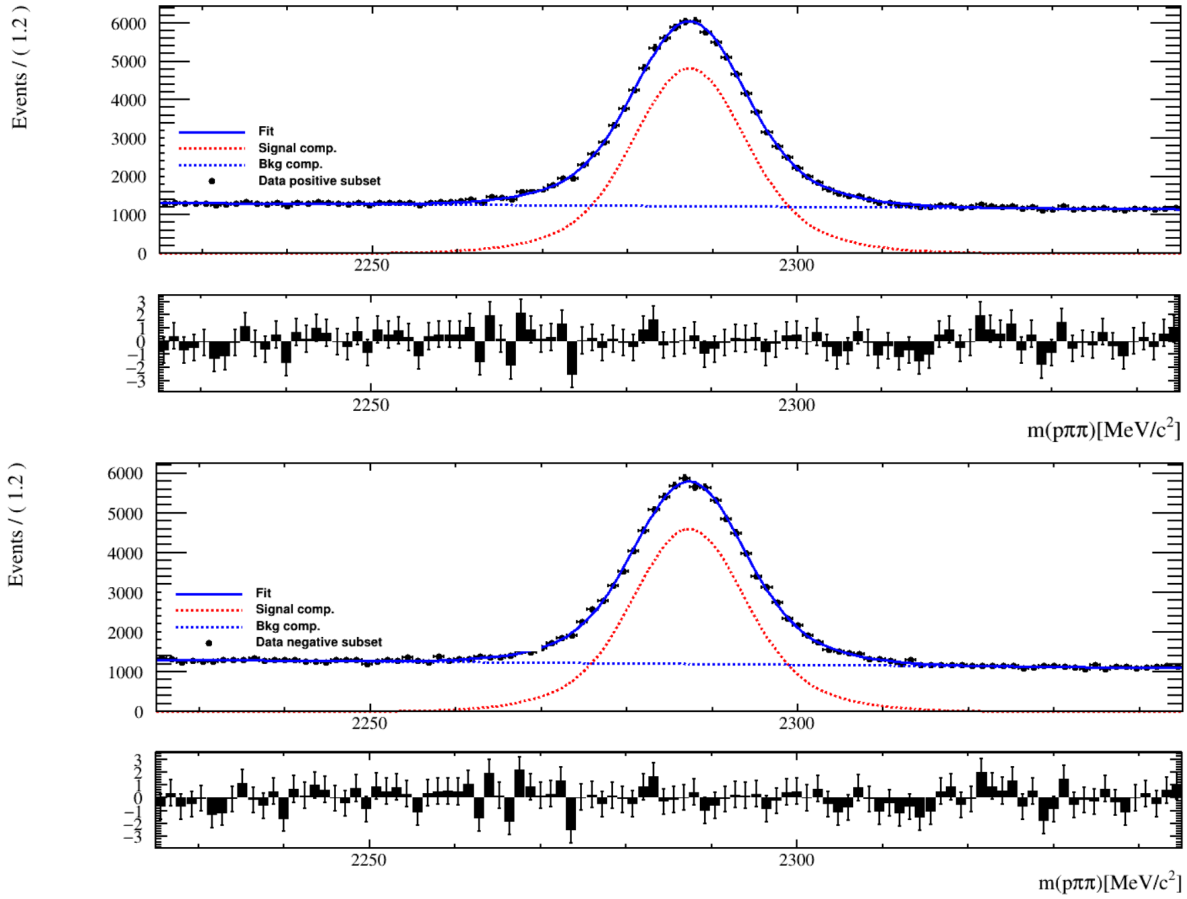

Figure 3.15: Invariant mass distribution of the two subsets of $p\pi\pi$ dataset, containing respectively positively charged protons (top) and negatively charged anti-protons (bottom). The fits (blue lines) used for the determination of weighted raw asymmetry are superimposed to data.

Conclusions

In the present thesis work CP violation in the semileptonic decays of the charm baryon Λ_c^+ has been investigated. This kind of measurements is crucial because they could exhibit discrepancies from predictions made according to the Standard Model. The analysis used Run 2 data, collected by the LHCb experiment in 2016, obtained from proton-proton collisions at center-of-mass energies $\sqrt{s} = 13$ TeV, with an integrated luminosity of 0.82 fb^{-1} and magnet down polarity. The two decay channels $\Lambda_c^+ \to p + K^+ + K^-$ and $\Lambda_c^+ \to p + \pi^+ + \pi^-$ have been taken into consideration, with the purpose of measuring the difference of CP violation in the two decay channels, ΔA_{CP}^{wgt}. Via a re-weighting procedure it was possible to get rid of the nuisance asymmetries coming from production and detection processes. The value obtained is

$$\Delta A_{CP}^{wgt} = (-0.2 \pm 0.9)\%, \tag{3.27}$$

where only the statistical uncertainty is reported. the result is compatible with zero and with the Run 1 measurements. However, this measurement is the result of a preliminary analysis, hence it does not represent a proof of the absence of CP violation in the decay channels at issue. The dataset used was only a small portion of Run 2 data, but it is already competitive with Run 1 measurements which have statistical uncertainty of 0.91% [12]. More statistics can be added to reduce uncertainties and more sophisticated techniques can be applied in the selection step. In the future, the full Run 2 dataset will be analyzed, together with Run 3 data, to further reduce the statistical uncertainty.

Bibliography

[1] Andrew J. Larkoski. *Elementary Particle Physics*. Cambridge University Press, 2019.

[2] E. Noether. "Invariante Variationsprobleme". In: *Nachrichten von der Gesellschaft der Wissenschaften zu Göttingen. Mathematisch-Physikalische Klasse* (1918).

[3] Alessandro Bettini. *Introduction to Elementary Particle Physics*. Cambridge University Press, 2008.

[4] T. D. Lee and C. N. Yang. "Question of Parity Conservation in Weak Interactions". In: *Physical Review* (1956).

[5] Nicola Semprini Cesari. "Fisica Nucleare e Subnucleare". Note del corso di Fisica Nucleare e Subnucleare A.A. 2023-2024.

[6] C. S. Wu et at. "Experimental Test of Parity Conservation in Beta Decay". In: *Physical Review* (1957).

[7] Leon M.Lederman Richard L. Garwin and Marcel Weinrich. "Observation of the Failure of Conservation of Parity and Charge Conjugation in Meson Decays: the Magnetic Moment of the Free Muon". In: *Physical Review* (1957).

[8] Donald H. Perkins. *Introduction to High Energy Physics*. Cambridge University Press, 2000.

[9] A. Pich. "CP Violation". In: *CERN Server* (1993).

[10] Marco Sozzi and Italo Mannelli. "Measurements of direct CP violation". In: *La Rivista del Nuovo Cimento* (2003).

[11] The LHCb Collaboration. "The LHCb Detector at the LHC". In: *Journal of Instrumentation* (2008).

[12] LHCb Collaboration. "A measurement of the CP asymmetry difference between $\Lambda c+\rightarrow$ pK- K and pπ- π decays". In: ().